https://doi.org/10.1093/plphys/kiad642 PLANT PHYSIOLOGY 2023: 00: 1–20

Plant Physiology®

Research Article

OROSOMUCOID PROTEIN 1 regulation of sphingolipid synthesis is required for nodulation in *Aeschynomene evenia*

Nico Nouwen,[1] **Marjorie Pervent**,[2] **Franck El M'Chirgui**,[1] **Frédérique Tellier**,[3] **Maëlle Rios**,[1] **Natasha Horta Araújo**,[1] **Christophe Klopp**,[4] **Frédéric Gressent**[2,†] **and Jean-François Arrighi**[1,*,†]

1 Plant Health Institute of Montpellier (PHIM), IRD, UMR Univ Montpellier/IRD/SupAgro/INRAE/CIRAD, TA-A82/J Campus de Baillarguet, 34398 Montpellier, France
2 Plant Health Institute of Montpellier (PHIM), INRAE, UMR Univ Montpellier/IRD/SupAgro/INRAE/CIRAD, TA-A82/J Campus de Baillarguet, 34398 Montpellier, France
3 Institut Jean-Pierre Bourgin (IJPB), INRAE, AgroParisTech, Université Paris-Saclay, 78000 Versailles, France
4 Plateforme Bioinformatique Genotoul, BioinfoMics, UR875 Biométrie et Intelligence Artificielle, INRAE, 31326 Castanet-Tolosan, France

*Author for correspondence: jean-francois.arrighi@ird.fr
†Senior authors.
The author responsible for distribution of materials integral to the findings presented in this article in accordance with the policy described in the Instructions for Authors (https://academic.oup.com/plphys/pages/General-Instructions) is: Jean-François Arrighi (jean-francois.arrighi@ird.fr).

Abstract

Legumes establish symbiotic interactions with nitrogen-fixing rhizobia that are accommodated in root-derived organs known as nodules. Rhizobial recognition triggers a plant symbiotic signaling pathway that activates 2 coordinated processes: infection and nodule organogenesis. How these processes are orchestrated in legume species utilizing intercellular infection and lateral root base nodulation remains elusive. Here, we show that *Aeschynomene evenia* OROSOMUCOID PROTEIN 1 (AeORM1), a key regulator of sphingolipid biosynthesis, is required for nodule formation. Using *A. evenia orm1* mutants, we demonstrate that alterations in AeORM1 function trigger numerous early aborted nodules, defense-like reactions, and shorter lateral roots. Accordingly, *AeORM1* is expressed during lateral root initiation and elongation, including at lateral root bases where nodule primordium form in the presence of symbiotic bradyrhizobia. Sphingolipidomics revealed that mutations in *AeORM1* lead to sphingolipid overaccumulation in roots relative to the wild type, particularly for very long-chain fatty acid-containing ceramides. Taken together, our findings reveal that AeORM1-regulated sphingolipid homeostasis is essential for rhizobial infection and nodule organogenesis, as well as for lateral root development in *A. evenia*.

Introduction

Legumes have the ability to establish a nitrogen-fixing symbiosis with bacteria collectively named rhizobia. They form specific root organs, the nodules, where rhizobia are housed to convert atmospheric dinitrogen into nitrogen organic compound in exchange for supply of carbon sources. In most rhizobium–legume interactions, nodulation occurs in a susceptible root zone with developing root hairs. Compatible rhizobia colonize the root hair surface and induce their curling to entrap a microbial colony in an infection chamber from which an infection thread develops. This tubular structure guides rhizobia to the nodule primordium that is distantly formed in the root cortex and where they are released. Bacterial accommodation is accompanied with their

Received October 06, 2023. Accepted October 31, 2023. Advance access publication December 1, 2023

differentiation into bacteroids that are dedicated to nitrogen fixation (Roy et al. 2020).

The molecular basis of the rhizobial symbiosis has been well studied in 2 temperate model legumes, Medicago (*Medicago truncatula*) and Lotus (*Lotus japonicus*), in which many nodulation genes have been identified. This symbiosis hinges on the recognition of rhizobial Nod factors by specific plasma membrane-localized lysin motif–receptor-like kinases. In turn, this recognition triggers a Nod signaling pathway leading to the activation of a network of nuclear transcription factors that induce the expression of symbiotic genes orchestrating the infection process and nodule organogenesis. Among them, nodule inception (NIN) was shown to play an important role in the transition of the nodule into a nitrogen-fixing state (Roy et al. 2020; Feng et al. 2021). These gene discoveries provided valuable information on the molecular mechanisms involved in rhizobial symbiosis, among which (i) part of the signaling and infection genes are also involved in the more ancient endomycorrhizal symbiosis (Gobbato 2015), (ii) the infection thread polarized growth involves a multiprotein infectosome complex linked to vesicle trafficking and the cytoskeleton (Liu et al. 2019; Lace et al. 2023), (iii) several plant genes are required to prevent defense reactions in nodules (Berrabah et al. 2019, and (iv) the developmental program of nodules overlaps with lateral roots (Schiessl et al. 2019; Soyano et al. 2019).

Although the above-described symbiotic mechanisms are likely representative of what occurs in many legume species, the legume family is huge and diverse (~20,000 species), and substantial variations on the theme of nodulation have been described. As example, in *Aeschynomene* species, root nodules form exclusively at a lateral root base (LRB) where a rosette of axillary root hairs is present. Bradyrhizobia enter the root at the base of these axillary root hairs and subsequently progress intercellularly in the root cortex. Eventually, the bacteria are endocyted by a few cortical cells that start to divide repeatedly to give rise to the nodule (Bonaldi et al. 2011). LRB nodulation is also found in other legume species like peanut (*Arachis hypogaea*) and *Sesbania rostrata* (Capoen et al. 2010; Sharma et al. 2020), and in 25% of the legume genera, rhizobial infection occurs via intercellular penetration with peanut as most known example (Quilbé, Montiel, et al. 2022). An even more rare variation is found in approximately 20 *Aeschynomene* species that interact symbiotically with photosynthetic *Bradyrhizobium* strains. In these species, symbiosis occurs without Nod factor recognition (Giraud et al. 2007; Chaintreuil et al. 2018). In that case, LRB nodulation-associated axillary root hairs and intercellular infection show specific adaptations that likely facilitate the so-called Nod-independent symbiosis (Bonaldi et al. 2011).

The recent release of the *Aeschynomene evenia* genome and a collection of EMS-induced nodulation mutants has positioned it as a valuable model plant to study these nodulation features (Quilbé et al. 2021; Quilbé, Montiel, et al. 2022; Quilbé, Nouwen, et al. 2022). Such analysis is predicted to enable the identification of additional symbiotic mechanisms and to complement the information on nodulation as obtained with the historical model legumes. Initial genetic studies using *A. evenia* mutants demonstrated the conservation of several genes of the symbiotic signaling pathway, *AePollux*, *Ca^{2+}/calmodulin-dependent kinase* (*AeCCaMK*), *AeCyclops*, *nodulation signaling pathway 2* (*AeNSP2*), and *AeNIN* but not of those coding for the upstream Nod factor receptors. The discovery of *cysteine-rich receptor-like kinase* (*AeCRK*), encoding a receptor-like kinase required for symbiosis, also presented an important avenue to further investigate how the Nod-independent symbiosis is activated (Quilbé et al. 2021). Further analyses revealed that these genes intervened during different steps of intercellular infection and that AeNSP2 has an additional function in controlling axillary root hair formation at LRBs, which constitute bradyrhizobia-colonized infection sites in *A. evenia* (Quilbé, Nouwen, et al. 2022).

Thus, although progress has been made in the identification of genes required for the activation of Nod-independent symbiotic and intercellular infection in *A. evenia*, our mechanistic understanding of intercellular infection and LRB nodulation remains in its infancy. In this study, we reported the mutant-based identification and functional characterization of the *A. evenia* OROSOMUCOID PROTEIN 1 (*AeORM1*) gene predicted to encode an orosomucoid (ORM) protein. ORM proteins are negative regulators of sphingolipid synthesis by inhibiting the activity of the serine palmitoyltransferase (SPT) (Li et al. 2016). Their regulatory role is pivotal since sphingolipids are important players in membrane structure and dynamics; they act also as bioactive molecules and are involved in a wide range of biological processes (Kimberlin et al. 2016). In *A. evenia*, alteration of ORM function resulted in shorter lateral roots and, in the presence of *Bradyrhizobium*, in early nodule abortion accompanied with defense-like responses, in accordance with a gene expression during nodule and lateral root formation. We also demonstrated that *ORM* mutations led to substantial modifications in sphingolipid composition in roots. These findings strongly suggest that ORM regulation of sphingolipid homeostasis plays a key role during nodule formation and further links nodule development to lateral root development in *A. evenia*.

Results

A. evenia ORM1 gene is required for rhizobial symbiosis

To uncover the molecular mechanisms underpinning the original nodulation properties found in *A. evenia*, we recently screened an EMS-mutagenized population for defects in nodule formation with the photosynthetic *Bradyrhizobium* strain ORS278 (Quilbé et al. 2021). Three nodulation mutants named P35, Q33, and AG2 were isolated based on nitrogen starvation symptoms (i.e. underdeveloped plants with yellowing leaves) that were similar to those observed for Nod$^-$ (no nodule) mutants such as *ccamk-3* (Fig. 1A). In

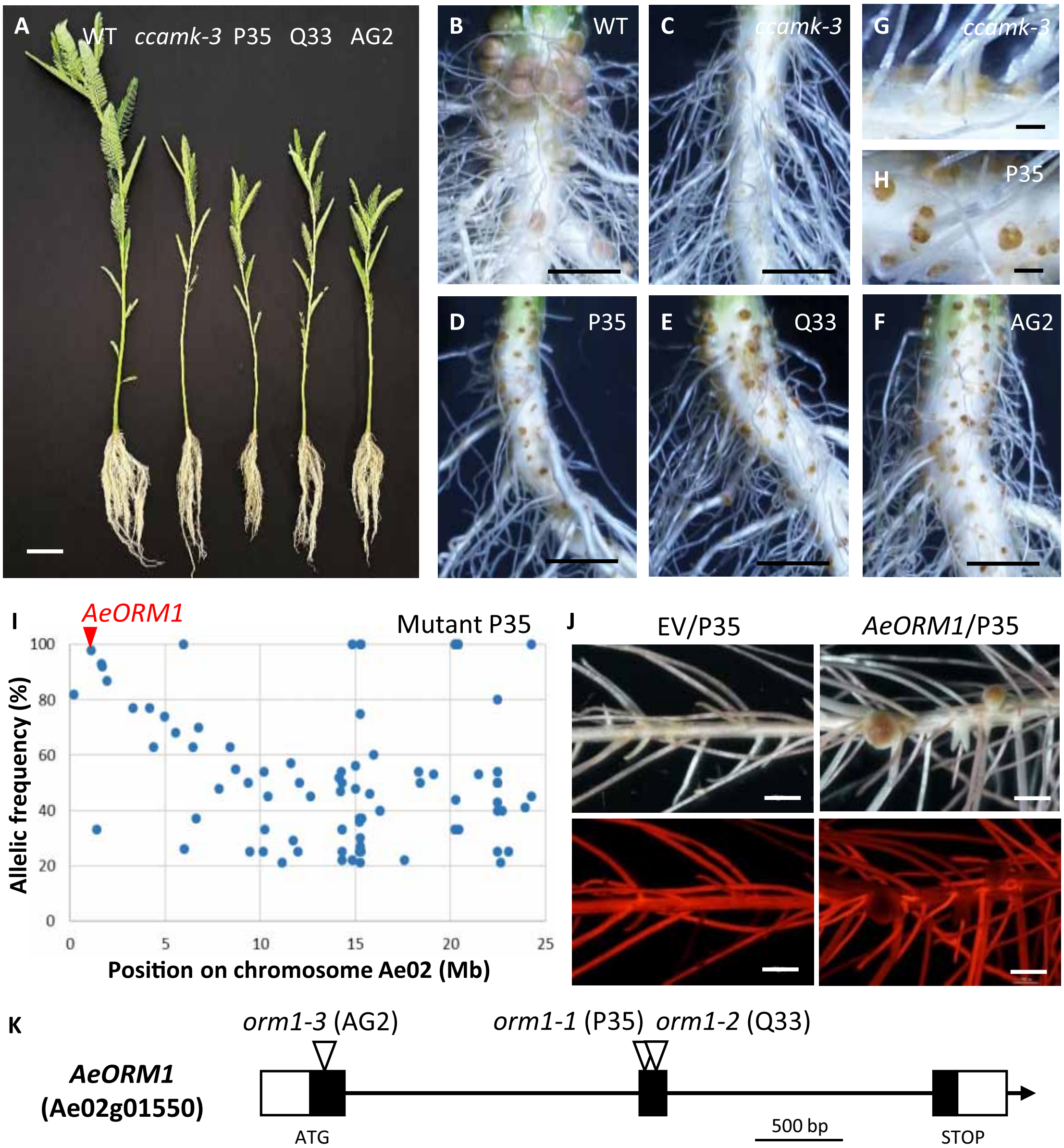

Figure 1. Mutations in *AeORM1* disrupt nodule formation and cause defense-like reactions. **A)** Growth phenotype of WT, *ccamk-3*, and P35, Q33, and AG2 mutant plants grown inoculated with *Bradyrhizobium* strain ORS278 and grown for 28 d in greenhouse conditions. Bar = 5 cm. **B to H)** Symbiotic phenotype of roots from plants shown in **A)**. Root of the WT carries pink nodules **B)**, while *ccamk-3* root is completely noduleless **C)** and the P35 **D)**, Q33 **E)**, and AG2 **F)** mutant roots display numerous brown spots at nodulation sites. Upper right panel shows a zoom of nodulation sites on *ccamk-3* **G)** and the P35 **H)** mutant roots. Bars = 5 mm **B to H)** or 500 μM **G to H)**. **I)** Frequency of the EMS-induced mutant alleles in bulks of backcrossed F_2 mutant plants of the P35 mutant as obtained by the mapping-by-sequencing approach. The single-nucleotide polymorphism representing the putative causal mutation is indicated by the arrow head (AF = 98%). **J)** Functional complementation assays. Transgenic hairy roots of *orm1-1* mutant plant containing the empty vector remain noduleless, whereas hairy roots containing the ProAeORM1-AeORM1 construct contain nodules at 28 dpi. (Upper panels) Bright field images of hairy roots and the (lower panels) epifluorescent microscopic images showing DsRed expression in the same transgenic roots. Bars = 2 mm. **K)** Structure of the *AeORM1* gene and positions of the EMS mutations identified in the P35 (*orm1-1*), Q33 (*orm1-2*), and AG2 (*orm1-3*) mutants. White boxes correspond to UTR regions and black boxes to exons, and arrow heads indicate locations of the mutations.

contrast to the wild-type (WT) line that produced pink-colored nodules and the completely noduleless *ccamk-3* mutant, the roots of P35, Q33, and AG2 mutant plants contained numerous brown spots at the base of lateral roots (Fig. 1, B to F). While the base of lateral roots of the *ccamk-3* mutant exhibited only the typical orange crowns of axillary root hairs, in the 3 newly analyzed mutants, the brown spots were round-shaped bumps, suggesting early abortion of nodule formation associated with defense-like pigment accumulation (Fig. 1, G and H).

F_2 progenies generated from crosses with the WT line segregated in a 3:1 ratio of plants with pink nodules to plants with only brown spots, suggesting that each mutation is monogenic and recessive (Supplemental Table S1). To identify the mutations causing this nodulation phenotype, we conducted a mapping-by-sequencing approach by sequencing pooled DNAs from mutant plants within the segregating F_2 populations. For the 3 mutants, a genetic linkage was identified at the same location near the top of the Ae02 chromosome (Fig. 1I; Supplemental Fig. S1). Closer inspection of this region revealed the presence of distinct mutations in the Ae02g01550 gene with a mutant allelic frequency of 98%, 98%, and 82% for the P35, Q33, and AG2 mutants, respectively (Supplemental Table S1). Functional annotation of the Ae02g01550 gene indicated that it is predicted to encode an ORM protein. ORM proteins are known to be localized in the endoplasmic reticulum (ER) where they act as major negative regulators of sphingolipid biosynthesis in plants and other eukaryotes (Kimberlin et al. 2016; Li et al. 2016). Therefore, we named this candidate gene *AeORM1*. To validate the *AeORM1* gene, allelism tests were performed by crossing the 3 mutants between them (Supplemental Table S2). All the F_1 plants produced brown spots after inoculation with *Bradyrhizobium* ORS278 strain. In addition, the full-length WT coding sequence (CDS) was cloned with its native promoter region (i.e. ∼2.1-kb upstream of the predicted start codon) and expressed using the hairy root transformation protocol in roots of P35 plants. In contrast to the P35 plants transformed with the empty vector that were completely noduleless, nodules readily developed on the complemented root systems after inoculation with *Bradyrhizobium* ORS278 (Fig. 1J, Supplemental Table S3). Taken together, these results unambiguously indicate that the mutations in *AeORM1* are responsible for the nodulation phenotype. Accordingly, we designated the alleles in the P35, Q33, and AG2 mutants *orm1-1*, *orm1-2*, and *orm1-3*, respectively. In the 3 exon-containing *AeORM1* genes, *orm1-3* mutation falls in Exon 1 while the *orm1-1* and *orm1-2* mutations are located in Exon 2 (Fig. 1K; Supplemental Table S1).

AeORM1 belongs to a small family of highly conserved genes

To our knowledge, the involvement of *ORM* genes in rhizobial symbiosis has not yet been reported. This prompted us to characterize the *ORM* gene family in legumes by searching for *AeORM1* homologs in 11 Papilionoideae and 2 Caesalpinioideae species for which the genome has been completely sequenced. *Arabidopsis* (*Arabidopsis thaliana*) and rice (*Oryza sativa*) *ORM* genes were included for comparison. One to four *ORM* homolog genes were retrieved for each considered species. The first phylogenetic analysis based on aligned protein sequences produced a tree topology that was completely inconsistent due to too low variation in these sequences (detailed thereafter). Therefore, we reiterated this analysis by using alignment of nucleotide sequences. In the resulting phylogenetic tree, *Arabidopsis* and rice *ORM* genes form 2 independent clades while legume *ORM* genes are organized in 3 clusters (Fig. 2A). One contained Caesalpinioideae genes and the 2 others had Papilionoideae genes. Interestingly, *AeORM1* clusters with *ORM1* representatives from all other Papilionoideae, forming the ORM1 clade. *A. evenia* contains a second gene copy of *ORM* gene that we named *AeORM2*. This copy has only counterparts in *Arachis* spp. with whom it forms a separate cluster which we named the ORM2 clade. Synteny analysis confirmed orthologous and paralogous relationships of *ORM* genes among Papilionoideae species, reinforcing the idea that the ORM1 and ORM2 clades result from the polyploidy event at the base of Papilionoideae (Supplemental Fig. S2) (Li et al. 2013). So, while only dalbergioid legumes seem to have retained the duplicated *ORM* copies (such as *A. evenia*), others have only preserved the *ORM1* copy (such as *M. truncatula* and *L. japonicus*). More recent gene or whole-genome duplications are likely responsible for variations in gene copy numbers as found in different species (e.g. soybean [*Glycine max*] and *A. hypogaea*).

Sequence alignment of the predicted ORM proteins revealed that they are almost all 157 amino acid (AA) long (Supplemental Fig. S3). Another striking feature was that these ORM proteins are highly conserved in their sequence throughout the plant kingdom. Indeed, AeORM1 and AeORM2 share 89.2% identity while AeORM1 shares 93% identity with the *M. truncatula* ORM protein and still an 84.1% identity with the more distantly related rice ORM proteins. Similar to *Arabidopsis* ORM proteins, legume ORM proteins are predicted to have 4 transmembrane domains, typically containing hydrophobic and neutral AAs while remaining sequences are enriched in hydrophile AAs (Fig. 2B). Interestingly, the mutations identified in the 3 *A. evenia orm1* mutants lead to AA substitutions in conserved residues of the first transmembrane domain (*orm1-3*: Gly25Asp) and the central loop (*orm1-1*: Pro75Leu and *orm1-2*: Gly95Arg) (Fig. 2B). The drastically altered nodulation phenotype of the *orm1* mutants strongly indicates that these AA substitutions are detrimental for ORM activity.

AeORM1 expression is associated with lateral root and nodule development

To get information on the potential involvements of the 2 *ORM* genes in *A. evenia*, their transcript levels were analyzed in the different plant organs and during symbiotic interactions. Both genes were found to be expressed ubiquitously in stems, leaves, flowers, pods, roots, and during nodulation, based on the *A. evenia* Gene Atlas (Supplemental Fig. S4, A and B). *AeORM1* expression levels appeared to be ∼30% higher than those of *AeORM2* in all conditions, except in flowers. To confirm and extend the *A. evenia* Gene Atlas data, reverse transcription quantitative PCR (RT-qPCR) analysis was conducted on RNA isolated from WT roots inoculated or not with *Bradyrhizobium* strain ORS278 (for nodulation) and

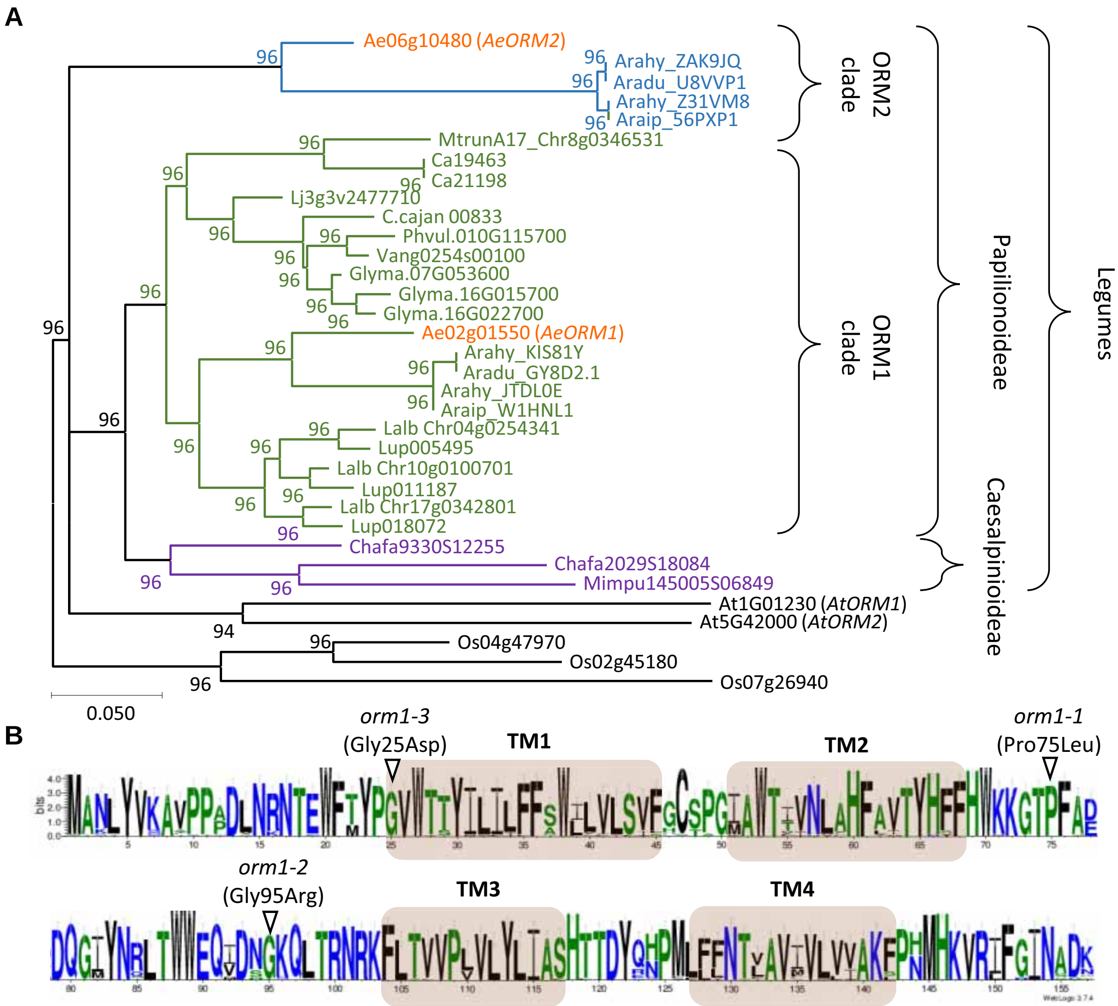

Figure 2. *AeORM1* is part of a highly conserved gene family. **A)** Maximum likelihood tree of plant ORM genes based on MUSCLE nucleotide alignment with 1,000 bootstrap values. Selected species are as follows: *A. evenia* (Ae), *A. thaliana* (AT), *A. hypogaea* (Arahy), *Arachis duranensis* (Aradu), *Arachis ipaiensis* (Araip), *Cajanus cajan* (C. cajan), *Chamaecrista fasciculata* (Chafa), *Cicer arietinum* (Ca), *G. max* (Glyma), *Lupinus albus* (Lalb), *Lupinus angustifolius* (Lup), *L. japonicus* (Lj), *M. truncatula* (Mtrun), *Mimosa pudica* (Mimpu), *O. sativa* (Os), *Phaseolus vulgaris* (Phvul), and *Vigna angularis* (Vang). Within the legume family, Caesalpinioideae genes are in purple and Papilionoideae genes are in green and blue to highlight the presence of the ORM1 and ORM2 clades and those of *A. evenia* in orange. The bar represents the estimated nucleotide change per sequence position. **B)** Sequence logo for plant ORM proteins generated after a MUSCLE alignment of the predicted protein sequences of genes used in **A)** using the WebLogo software and showing the conserved AA residues. Blue, hydrophilic AAs; green, Neutral AAs; and black, hydrophobic AAs. Predicted transmembranes (TMs) are indicated by shaded boxes and AA changes resulting from the EMS mutations in *AeORM1* are indicated by arrow heads.

Rhizophagus irregularis (for mycorrhization). Similar expression patterns were observed for both genes during the 2 symbioses (Supplemental Fig. S4, C and D). These data suggested that *AeORM1* and *AeORM2* might act in concert and that *AeORM1*, in addition to nodulation, may have other roles in the development of *A. evenia* plants.

To analyze the spatial expression of the *AeORM1* gene, we fused the ~2.1-kb promoter region to the *GUS* reporter gene. This p*AeORM1-GUS* construct was used to transform WT *A. evenia* roots with *Agrobacterium rhizogenes*, and GUS activity was monitored in noninoculated and inoculated roots. In noninoculated roots, GUS staining was observed in lateral root primordia as found, in particular, in the younger part of the primary root (Fig. 3, A to C). Once emerged from the primary root, GUS staining was observed both at the base and tip of lateral roots (Fig. 3, D to F). After inoculation with *Bradyrhizobium* ORS278, enhanced GUS staining was observed at nodule primordium initiation sites located at LRBs and where both rhizobial infection and cell divisions occur (Fig. 3, G to K). When young nodules became apparent (i.e. at 4 d postinoculation [dpi]), GUS staining was observed in the region that surrounded the central infected tissue (Fig. 3L). GUS staining persisted in mature nodules (i.e. at 11 dpi). However, sectioning and examination of these nodules by light microscopy revealed specific expression of p*AeORM1-GUS* at the nodule base and in a few cell layers

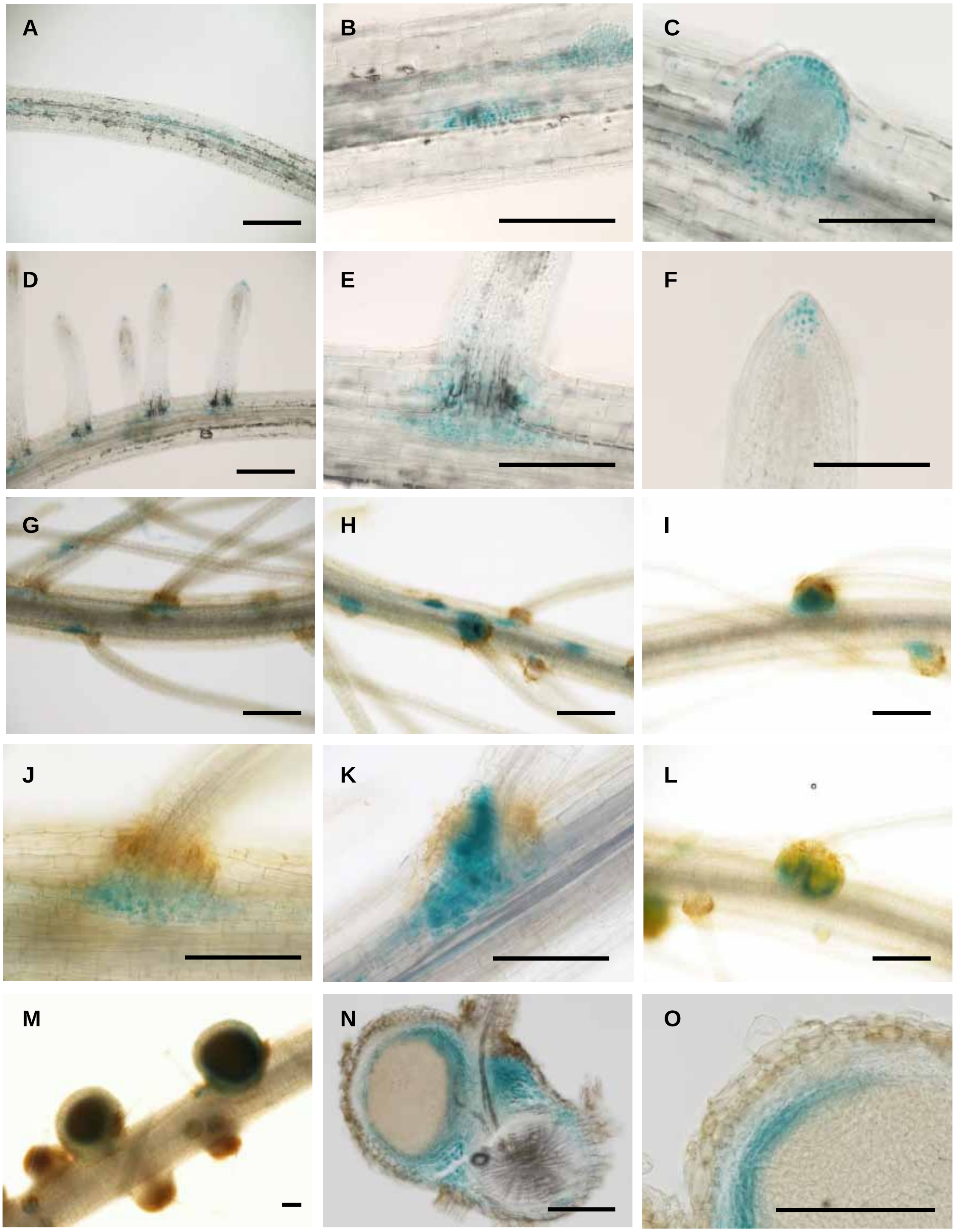

Figure 3. *AeORM1* is expressed during root and nodule initiation and development. Histochemical localization of GUS activity in *A. rhizogenes* roots of WT *A. evenia* transformed with proAeORM1-GUS. **A to F)** Noninoculated roots showing glucuronidase activity during lateral root initiation and development. **A)** Whole primary root, **B, C)** zoom on inner and emerging root primordia, **D)** whole primary root with elongating lateral roots, and **E, D)** base and apex of an elongating lateral root, respectively. Bars = 500 μm. **G to L)** Glucuronidase activity in roots 4 d after inoculation with B*radyrhizobium* ORS278. The sequential enlargement of the zone containing glucuronidase activity is shown in **G)**, **H)**, and **I)**, respectively, and zooms showing **J)** basal activity, **K)** nodule primordium-associated activity, and **L)** activity relocalization in young nodules. Bars = 500 μm. **M to O)** Glucuronidase activity in nodules at 11 dpi. **M)** Whole nodules showing intense blue coloration after staining roots with X-Gluc. **N)** Glucuronidase activity in a nodule section. **O)** Zoom in a nodule section showing glucuronidase activity in only plant cells at the periphery of the central infected tissue. Bars = 200 μm.

encircling the central nitrogen fixation zone (Fig. 3, M to O). Prolonged GUS staining of sectioned nodules never led to blue coloration of the central infected tissue.

Nodule formation is compromised in *orm1* mutants

To associate the *AeORM1* expression pattern during nodulation with the observed mutant phenotypes, we studied the nodulation kinetics of the 3 *orm1* mutants after inoculation with *Bradyrhizobium* strain ORS278 and analyzed their symbiotic alterations by light microscopy at different time points (7, 10, 14, and 21 dpi). In WT plants, mature nodules became slightly pink at 7 dpi, and this pink coloration intensified at later stages, an indication of leghemoglobin accumulation (Supplemental Fig. S5). In contrast, no nodules developed in the 3 *orm1* mutants. However macroscopic examination of root sections evidenced limited cell divisions at the base of some lateral roots, indicative of nodule initiation, and brown spots, likely a result of accumulation of defense-like pigments. These features were discrete and visible as soon as 7 dpi, but the presence of both bumps and brown spots was more pronounced at later time points (Supplemental Fig. S5). A more detailed analysis was performed using a GUS-tagged version of strain ORS78. At 10 dpi, examination of whole and sectioned roots showed that the brown spot-containing bumps were lobe shaped like during nodule formation in WT *A. evenia* (Arrighi et al. 2012), but a gradation in the development was observed in the different *orm1* mutant plants: with the *orm1-1* plants, only limited cell divisions were observed whereas *orm1-3* plants contained more round-shaped bumps (Fig. 4A). X-Gluc staining revealed that all 3 *orm1* mutants were colonized by bradyrhizobia. In this aspect, the *orm1-1* mutant was again the most severely affected with only a few inner infection pockets, while in *orm1-2* and *orm1-3* mutant plants, bumps with a central infected tissue were visible (Fig. 4A). Dark brown spots were located in the vicinity of infection pockets in the *orm1-1* mutant plants, and they were present in the form of more extended brownish areas in the outer and/or inner nodule tissues of both other *orm1* mutants (Fig. 4A).

Next, we examined the effect of mutation in *AeORM1* on the expression of several genes that were previously shown to be induced during the initiation of rhizobial symbiosis in *A. evenia*: *early nodulin 40* (*AeENOD40*), *AeCRK*, *symbiotic remorin 1* (*AeSymREM1*), *vapyrin* (*AeVPY*), *subtilase* (*AeSBT*), and *AeNIN* (Quilbé, Nouwen, et al. 2022). RT-qPCR analysis was used to assay their induction by *Bradyrhizobium* ORS278 in the *orm1-1* mutant that shows the earliest block in nodule formation. The expression of all analyzed genes is induced as soon as 2 dpi and shows a continuous increase in expression up to 7 dpi in WT plants (Fig. 4B). In contrast, in the *orm1-1* mutant, *AeENOD40* expression reached a maximum at 2 dpi and then decreased in the following points (4 to 7 dpi). A low induction of expression in early time points (2 to 4 dpi) and premature decrease in later time points (4 to 7 dpi) was observed for the *AeCRK*, *AeSymREM1*, *AeSBT*, and *AeNIN* genes (Fig. 4B). These altered expression patterns are consistent with the phenotypic symbiotic responses observed in the *orm1-1* mutant (i.e. limited cell divisions and infection). In contrast to the other analyzed genes, the induction of the *AeVPY* gene was completely impaired in the *orm1-1* mutant (Fig. 4B).

Defense-like reactions and altered rhizobial accommodation in *orm1* mutants

Since all 3 *orm1* mutants produce discrete bumps with brown pigmentation after infection with *Bradyrhizobium* ORS278, we wanted to characterize this pigmentation in more detail. In the first step, we made use of roots inoculated with *Bradyrhizobium* strain ORS278-GUS and that at 14 dpi were sectioned and stained with X-Gluc before microscopic observation. Brown pigmentation was visible within the bumps of all 3 *orm1* mutants, and also dark brown inner spots were observed in the *orm1-1* mutant (Supplemental Fig. S6A). Fluorescent microscopic analysis showed that the brown areas had a green fluorescence when using a green filter (GFP) but not the dark brown inner spots present in the *orm1-1* mutant (Supplemental Fig. S6B). Red fluorescent areas were also observed when using a red filter (mCherry), and although they showed some overlap with the green fluorescent areas, the red fluorescent areas were in general more extended within the bumps, suggesting that the brown pigmentations may correspond to different phenolic compounds (Supplemental Fig. S6C). Then, the presence of phenolic compounds in *orm1* bumps was confirmed using staining root sections with potassium permanganate/methylene blue. Precipitates of blue stain at sites of brown pigmentation were observed in all 3 *orm1* mutants and were completely absent in sections of the WT nodules (Fig. 5A). Finally, 3,3′-diaminobenzidine (DAB) staining revealed higher concentrations of H_2O_2 in regions where brown pigments accumulated in the *orm1* bumps, suggesting a concomitant alteration of redox status in these areas (Fig. 5B).

To determine to which extent the observed defense-like reactions are accompanied with defects in rhizobial colonization of symbiotic cells and rhizobial differentiation into bacteroids, *orm1* mutants were inoculated with a GFP-tagged version of the *Bradyrhizobium* strain ORS278 and at 14 dpi root sections were observed by confocal microscopy. Analysis of WT nodule sections revealed that the central tissue was largely occupied by infected cells packed with green fluorescent bacteria (Fig. 6A). In contrast, *orm1* bumps were characterized by infected plant cells that were unevenly filled and that contained less bacteria than the WT. Strong autofluorescence was visible both within and outside of the central tissue (Fig. 6, B to D). Mature nodules of the WT plants contained typical enlarged and spherical bacteroids while only elongated bacteria were observed in bumps of the 3 *orm1* mutants, suggesting an impaired differentiation process (Fig. 6, E to H). The block in bradyrhizobia differentiation associated with the nitrogen starvation symptoms of the plants, the early arrest in nodule development resulting in

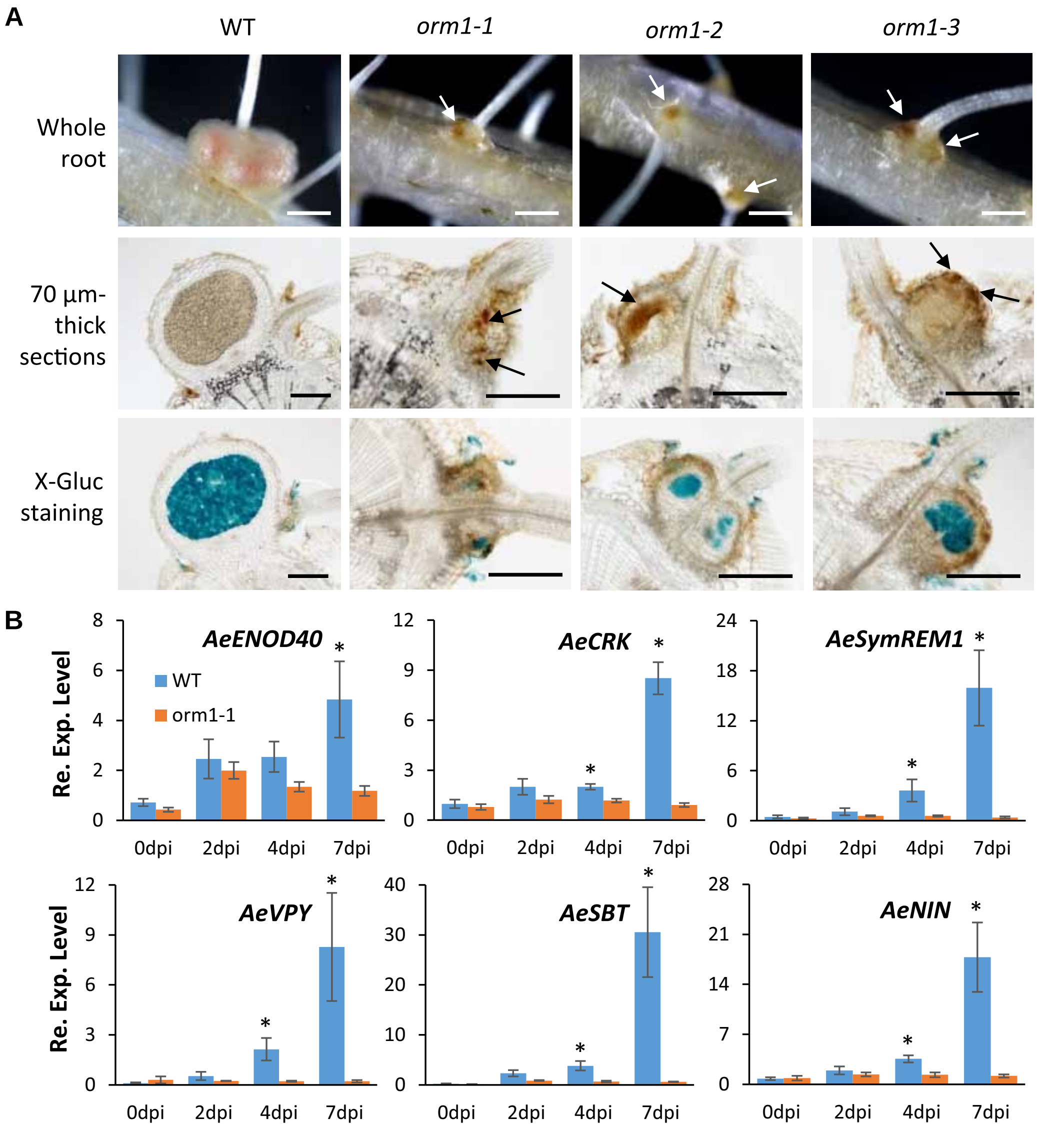

Figure 4. Mutations in *AeORM1* impair nodule development and alter symbiotic signaling. **A)** Nodule development in WT and *orm1* mutant plants at 10 dpi with *Bradyrhizobium* ORS278-GUS. Whole roots (upper panels) and 70-*µ*m-thick root sections before and after X-Gluc staining (middle and lower panels, respectively). Arrows point to the brown pigments visible in sections of *orm1* mutant roots. Bars = 250 *µ*m. Observations come from 2 experiments with 6 plants per line. **B)** Expression of early nodulation genes in WT and *orm1-1* mutant plants. Expression of *AeENOD40*, *AeCRK*, *AeSymREM1*, *AeVPY*, *AeSBT*, and *AeNIN* in plant roots was determined during nodulation kinetics with *Bradyrhizobium* ORS278 at 0, 2, 4, and 7 dpi by RT-qPCR analysis. Expression values were normalized using *AeEF1a* and *Ubiquitin* expression levels as standard. Means and SD were derived from 4 biological replicates, with 5 pooled plants per replicate, and asterisks above the bars represent statistically significant differences (Mann–Whitney test; $^*P < 0.05$).

bumps that were hardly visible by the naked eye and the absence of nitrogenase enzyme activity in acetylene reduction assays (Fig. 6, I to K).

AeORM1 is important for normal lateral root development

AeORM1 expression in nonsymbiotic organs suggested that the role of this gene might not be restricted to rhizobial symbiosis. When analyzing the symbiotic phenotype for the 3 allelic *orm1* lines using hydroponic growth conditions in the growth chamber, we noticed that young mutant plants have shorter lateral roots as compared to the WT plants. To avoid potential influences of age and nitrogen fixation on lateral root development, we assessed the root system architecture of the WT line and the 3 *orm1* mutants, cultured in liquid buffered nodulation medium (BNM) containing 0.5 mM KNO_3 for 10 d and without inoculation. Two out of the three *orm1* mutants had primary roots that were slightly shorter as compared to the WT plants while the lateral root number was found to be globally the same in all analyzed lines (Fig. 7, A and B). In contrast, significant decreases in

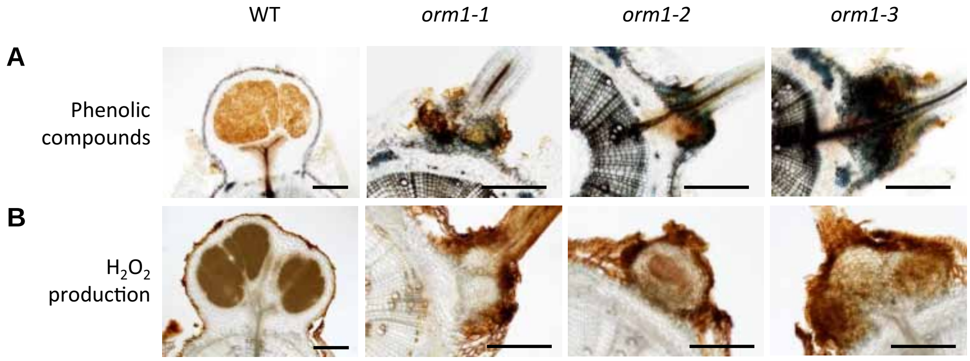

Figure 5. Mutations in *AeORM1* cause defense-like reactions. **A, B)** 70-μm-thick root or nodule sections of WT and *orm1* mutant plants at 14 dpi with *Bradyrhizobium* ORS278 strain. Bars = 250 μm. **A)** Staining of nodule sections of plants inoculated with *Bradyrhizobium* ORS278 with potassium permanganate ($KMnO_4$) and methylene blue. Blue staining indicates the presence of phenolic compounds in the plant tissue. **B)** Staining of nodule sections of plants inoculated with *Bradyrhizobium* ORS278 with DAB to detect hydrogen peroxyde (H_2O_2) production.

the lateral root length were found in all mutant lines relative to the WT, with the *orm1-1* mutant showing the most altered root phenotype (Fig. 7, C and D). Thus, *orm1* mutants have both a nodulation phenotype and an alteration in lateral root elongation. This suggests that *AeORM1* is involved in both lateral root and nodule development, in accordance with the observed expression pattern of this gene.

Mutations in *AeORM1* does not impair mycorrhization

As many genes important for rhizobial symbiosis are also involved in mycorrhizal symbiosis, we investigated the role of *AeORM1* in the formation of arbuscular mycorrhiza (AM). In the first experiment, roots of the WT line and 3 *orm1* mutants were inoculated with spores of *R. irregularis* and collected for analysis 6 wk later. Their observations revealed that similar to the WT plants, roots of the 3 *orm1* mutants contained fungal hyphae, arbuscules, and vesicles being conspicuous in the roots of all lines (Supplemental Fig. S7A). Mycorrhization frequency and intensity of the mutants were either similar or slightly higher relative to the WT (Supplemental Fig. S7B). To refine the analysis, we focused on the strongest allele mutant, *orm1-1*, and quantified the AM colonization again. At 6 wk postinoculation (wpi), the mycorrhization frequency and intensity of the mutant were slightly increased compared to the WT (Fig. 8, A and B). To further characterize AM symbiosis in *orm1* mutants, the expression of the marker genes *AeRAM1*, *AeVPY*, *AeSTR*, and *AeSBTM1* was next investigated by RT-qPCR. These plant genes were previously shown to be strongly induced by AM infection in *A. evenia* (Quilbé, Montiel, et al. 2022; Quilbé, Nouwen, et al. 2022). In the *orm1-1* mutant, the induction levels of all tested genes were similar to those in WT plants (Fig. 8C). Quantification of the presence of the *RiLSU* and *RiGADPH* genes (markers of fungal biomass) in the root tissue indicated that the abundance of *R. irregularis* in *orm1-1* roots was equal to the WT roots (Fig. 8C). Although it remains to be determinate whether the moderately increased mycorrhizal colonization level in the *orm1-1* mutant results from direct effect of the mutation in *AeORM1* or is a consequence of the altered root architecture, all 3 *omr1* mutants appear to be able to develop a functional mycorrhizal symbiosis.

Mutations in *AeORM1* alter sphingolipid contents in roots

ORM proteins act as major negative regulators of the first step of the sphingolipid biosynthetic pathway where the condensation of Ser with palmitoyl-CoA gives rise to long-chain bases (LCBs). These LCBs can be further modified and paired with structurally diverse fatty acids to produce ceramids (CERs) and hydroxyceramides (hCERs) that provide the backbone for more complex sphingolipids, including glucosylceramides (GlcCERs) and different glycosylinositolphosphoceramides (GIPCs) (Fig. 9A) (Alsiyabi et al. 2021).

As sphingolipids have not yet been investigated in *A. evenia*, we first set up a reference sphingolipidomic profiling for this species. To do so, we analyzed the major classes of sphingolipids in the roots of WT plants and compared roots grown in BNM containing either 0.5 or 5 mM KNO_3. Sphingolipid quantification on 4-wk-old WT roots revealed little to no differences between the low and high nitrogen conditions (Fig. 9, B to F). Then, we determined sphingolipid composition in roots and nodules following inoculation with *Bradyrhizobium* strain ORS278 of WT plants. Four weeks after inoculation, we excised the nodules from the roots and analyzed both organs. Sphingolipid amounts in uninoculated WT roots were similar to inoculated WT roots from which the nodules had been excised (Fig. 9, B to F). Moderate differences were seen in the CER, hCER, and GlcCER composition between WT roots and nodules (Fig. 9, B to D). More striking were the detected opposed variations for the GIPC pool, with NH_2GIPC (amino-GIPC) showing a 2-fold decrease and NHAcGIPC (acetylamino-GIPC) a 1.7-fold increase in WT nodules relative to WT roots (Fig. 9, E and F). As a result, NHAcGIPC constituted more

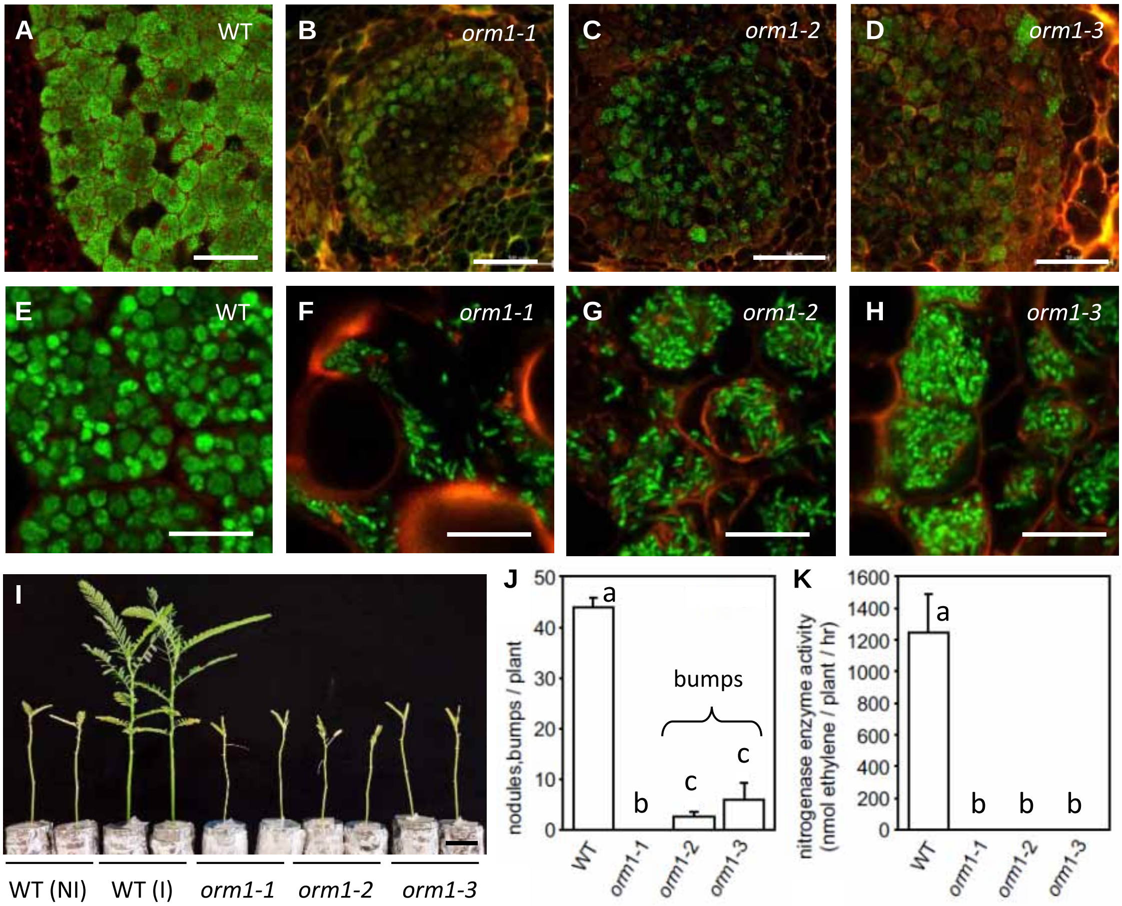

Figure 6. Mutations in *AeORM1* impair bacterial differentiation and nodule functioning. **A to D)** Confocal microscopic analysis of longitudinal 70-*µ*m-thick sections of nodules of WT **A)**, *orm1-1* **B)**, *orm1-2* **C)**, and *orm1-3* **D)** mutant plants inoculated with *Bradyrhizobium* ORS278-GFP at 14 dpi. Plant cell walls are visualized using their autofluorescent characteristics. Bars = 50 *µ*m. **E to H)** High magnification images of nodule sections showing the bacterial cell morphology in infected plant cells of the WT **E)**, *orm1-1* **F)**, *orm1-2* **G)**, and *orm1-3* **H)** mutant lines. At 14 dpi, bacteria are spherical in nodule cells of WT plants and elongated in infected cells of the *orm1* mutant plants. Bars = 10 *µ*m. **I)** Growth of noninoculated (NI) and inoculated (I) plants (aerial part) after cultivation under hydroponic condition in a growth chamber. Images were taken 21 d after inoculation with *Bradyrhizobium* ORS278. Bar = 1.5 cm. **J to K)** Number of bumps and nodules on plants **J)** and nitrogenase enzyme activity measured by the acetylene reduction assay **K)** of plants at 21 dpi. Error bars represent SD ($n = 6$). Different letters represent significant differences determined using a pairwise Wilcoxon test, $P < 0.05$.

than 75% of the total GIPC pool in WT nodules. Higher quantities of both NH_2GIPC and NHAcGIPC d18:0- and d18:1-h16:0 were found in nodules. However, most of the variations actually concerned the predominant NH_2GIPC and NHAcGIPC t18:0- and t18:1-h24:0 forms (Fig. 9, G to J).

To investigate the contribution of *AeORM1* in sphingolipid biosynthesis, we compared the major classes of sphingolipids present in the roots of the WT and 3 *orm1* mutant plants. The sphingolipid profiles of the *orm1* mutants showed an increased level in CER (*orm1-1*: ∼5-fold; *orm1-2*: ∼4-fold; *orm1-3*: ∼3-fold) as compared to the WT, which is specifically due to an overaccumulation of species containing trihydroxy LCB t18:0 and t18:1 (Fig. 10A). No significant quantitative differences were observed for the other sphingolipid categories (Fig. 10, B to E). Remarkably, the CER backbones containing very long-chain fatty acids (VLCFAs) (C22 to C26, the C24 fatty acid being the major one) exhibited a much more dramatic increase than CER containing long-chain fatty acids (C16 and C20) (Fig. 10, F to I). Overall, these findings indicated that the symbiotic and lateral root phenotypes of *orm1* mutants were associated with an overaccumulation of VLCFA-containing CERs in *A. evenia* roots.

Discussion

Using *A. evenia* mutants impaired in nodule formation, we identified the *AeORM1* gene that is predicted to encode an ORM protein. ORM proteins are key negative regulators of sphingolipids synthesis in eukaryotes and serve important functions in *Arabidopsis*, a nonsymbiotic plant, but a role for ORM proteins in the rhizobial symbiosis has so far never been reported. This gene discovery illustrates how research

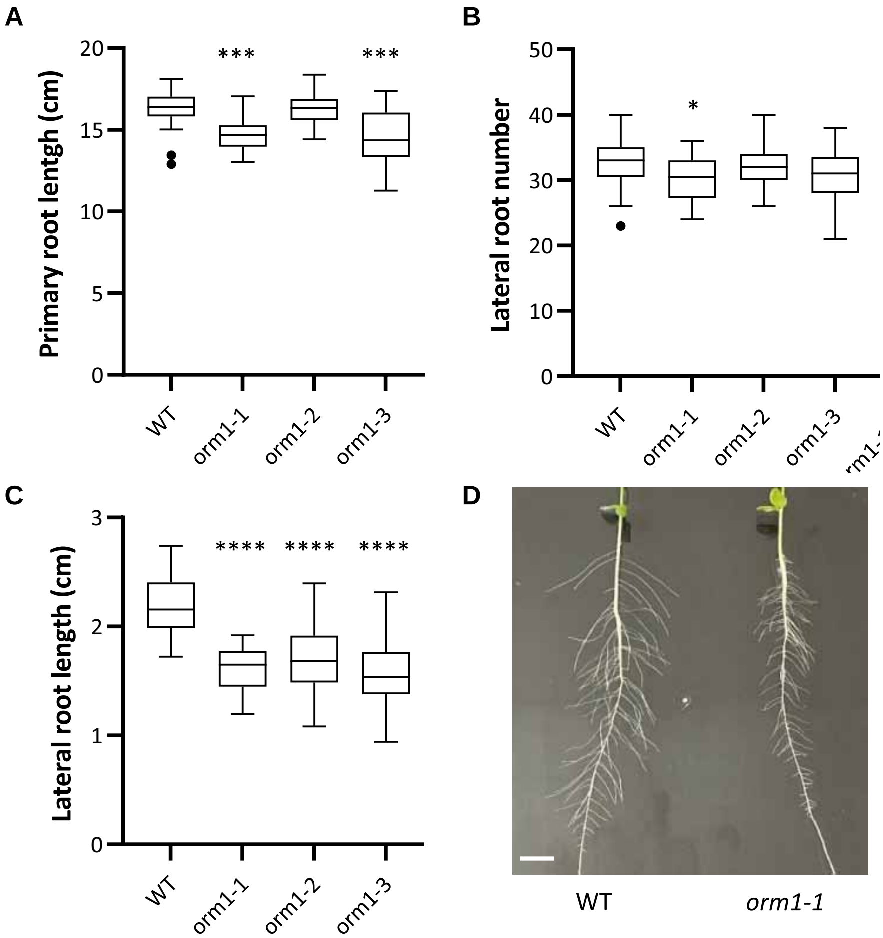

Figure 7. Lateral root development is reduced in *orm1* mutants. Analysis of the root system architecture of 10-d-old *A. evenia* WT and *orm1* mutant plants. **A to C)** Box plots showing the median (central segment), second to third quartiles (box), minimum and maximum ranges (whiskers), and outliers (single points) of measurement of **A)** primary root length, **B)** lateral root number on a segment of 3 cm in the upper part of the primary root, and **C)** lateral root length on the same segment of 3 cm as in **B)**. $^*P < 0.05$, $^{***}P < 0.001$, and $^{****}P < 0.0001$, significant differences between WT plants and each *orm1* mutant using a 1-way Kruskal–Wallis test. $n = 21$ (WT), 24 (*orm1-1*), 24 (*orm1-2*), and 17 (*orm1-3*). **D)** Images showing a primary root of a WT and *orm1-1* plant with emerging lateral roots. Bars = 1 cm.

on *A. evenia* nodulation is valuable to complement the information gained using historical model legumes. In contrast to the recently identified *AeCRK* gene, which is essential for symbiosis establishment in *A. evenia* and that has no obvious ortholog in *M. truncatula* and *L. japonicus* (Quilbé et al. 2021), *ORM* genes are present in all legume species, but in genetic screens in the historical model legumes, they have not been identified as important for nodulation. A reason for this could be that *A. evenia* constitutes a distinct genetic background. Indeed, while a single *ORM* gene copy is present in most legume species, including *M. truncatula* and *L. japonicus*, 2 paralogous genes are present in the syntenic position in *A. evenia*. Differential retention of paralogs that likely results from the ancestral WGD event in papilionoids has been repeatedly noticed in symbiotic genes. Notable instances include *Symbiosis Receptor-like Kinase 1&2* (*AeSYMRK1&2*), *Ethylene Responsive Factor Required for Nodulation 1&2* (*MtERN1&2*), and *Ethylene Insensitive 1&2* (*LjEIN1&2*) (Miyata et al. 2013; Yano et al. 2017; Quilbé et al. 2021). Given the central role of ORM proteins in plant development, the inactivation in single copy having legume species might be detrimental. In *Arabidopsis*, gene-edited *ORM* mutants yielded nonviable seeds, thereby impeding normal life cycle completion (Gonzalez-Solis et al. 2020). In *A. evenia*, the presence of 2 *ORM* paralogs might provide functional redundancy or specialization. This idea is supported by the observation that *A. evenia orm1* mutants are still able to develop correctly and produce fertile seeds. Testing mutants for the single *ORM* gene in *M. truncatula* or *L. japonicus*, and for *AeORM2*—either alone or in combination with *AeORM1*—would help solve these questions. Another possibility is that *ORM* genes have differential symbiotic involvements in legumes. *A. evenia* symbiosis differs at several points from those present in *M. truncatula* and *L. japonicus*. It has a Nod factor-independent activation and uses an intercellular infection and a LRB nodulation

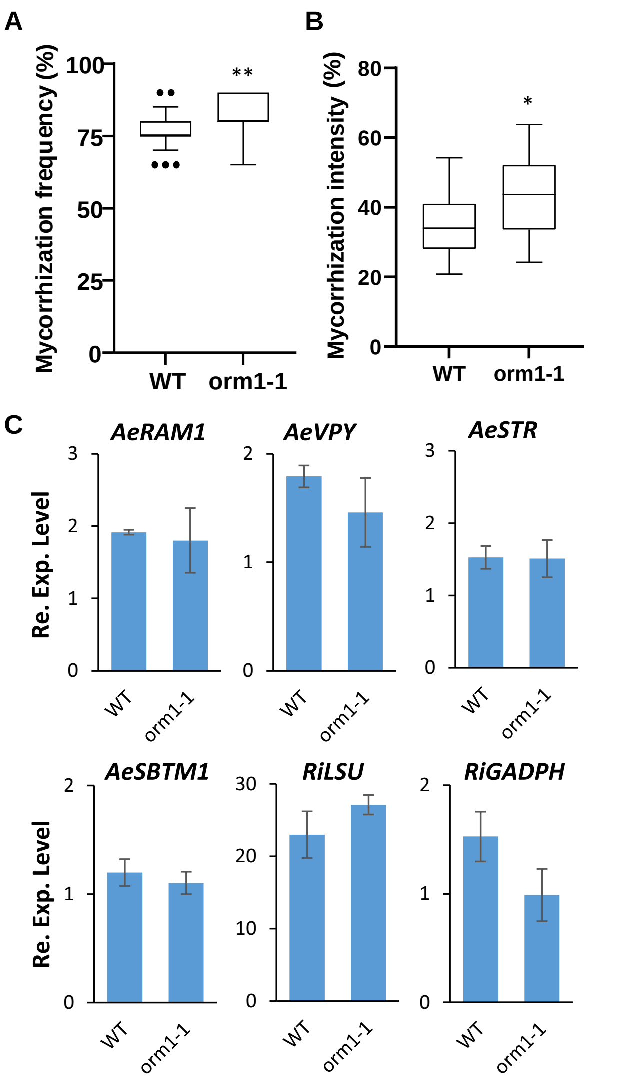

Figure 8. *AeORM1* does not impair mycorrhization. **A)** Mycorrhization frequency and **B**) intensity both expressed in % in WT and *orm1-1* mutant plants. Box plots show median (central segment), second to third quartiles (box), minimum and maximum ranges (whiskers), and outliers (single points). Data are from 4 biological repeats, each with 6 plants/line. $^{*}P < 0.05$ and $^{**}P < 0.001$, significant differences between WT and *orm1-1* mutant plants using a Mann–Whitney test. **C)** Expression of mycorrhization-induced genes in WT and *orm1-1* mutant plants. Expression of *AeRAM1*, *AeVPY*, *AeSTR*, *AeVPY*, *AeSBTM1*, and the 2 fungal genes *RiLSU* and *RiGADPH* was determined by RT-qPCR using plant roots inoculated with *R. irregularis* and cultivated for 6 wk. Expression values were normalized using *AeEF1a* and *Ubiquitin* expression levels as standard. Means and SD were derived from 3 biological replicates. For each analyzed gene, no statistically significant differences were observed between WT and *orm1-1* mutant plants (Mann–Whitney test; $P < 0.05$).

process (Bonaldi et al. 2011; Quilbé et al. 2021; Quilbé, Nouwen, et al. 2022). Interestingly, analysis of the *AeORM1* expression pattern revealed a constitutive expression at LRBs where rhizobial infection and nodule formation occur. This information complements the one recently obtained in another LRB-nodulating legume, *A. hypogaea*, for which the expression of the symbiotic genes *AhNIN* and *AhCYCLOPS* was found to be induced specifically at LRBs upon rhizobial inoculation (Bhattacharjee et al. 2022). In addition, the early abortion of nodule development in the *A. evenia orm1* mutants shows that *AeORM1* is essential for LRB nodulation.

The 3 *orm1* mutants displayed a gradation in their bump phenotype that was caused by AA substitutions at the conserved residues. This suggested that they possibly represent knockdown mutations and this questions if a more drastic symbiotic phenotype could be obtained in a knockout mutant. Pending this question, the observed bumps in the 3 *orm1* mutants differed from those previously described in certain *A. evenia* nodulation mutants for the *AePOLLUX*, *AeCYCLOPS*, and *AeCRK* genes (Quilbé, Nouwen, et al. 2022) in being numerous and by having visible brown spots. In all 3 mutants, infection of plant cells by *Bradyrhizobium* clearly differed from WT plants both quantitatively (infected cells were less filled with bacteria) and qualitatively (the bacteria were not differentiated into bacteroids). Because nodule formation is triggered in the *orm1* mutants but rapidly arrested, we hypothesize that *AeORM1* is required for nodule development and not for early perception of bradyrhizobia or NIN. This conclusion is supported by a RT-qPCR analysis showing the partial induction of symbiotic genes following the inoculation of an *orm1* mutant with *Bradyrhizobium*, with the exception of the infection marker *AeVPY*. Interestingly, expression studies using a p*AeORM1*-GUS construct showed a specific expression of *AeORM1* in cells at the base of lateral roots where nodule primordium form following the rhizobial infection. However, in nitrogen-fixing nodules, *AeORM1* expression was not associated with bacteroid-containing nodule cells. Based on these observations, we hypothesize that *AeORM1* is important for bacterial infection and nodule structure formation, acting downstream of NIN but prior to nodule differentiation. If right, *AeORM1* could represent a nodule emergence stage-specific regulator as described for *NF-YA1* (*Nuclear Factor YA1*) in *M. truncatula* and *L. japonicus* (Laporte et al. 2014; Hossain et al. 2016; Shrestha et al. 2021). The presence of brown spots in aborted nodules was found to correspond to the accumulation of phenolic compounds along with high concentrations of H_2O_2. They are reminiscent to those observed in mutants of different genes: *MtNAD1* (*Nodules with Activated Defense 1*), *MtDNF2* (*Does Not Fix Nitrogen 2*), *MtSymCRK* (*Symbiotic Cysteine-rich Receptor-like Kinase*), *MtNIP/LATD* (*Numerous Infections and Polyphenolics/Lateral root-organ Defective*), *MtRSD* (*Regulator of Symbiosome Differentiation*), and *MtNDP1* (*Nodule-Specific PLAT Domain Protein 1*) (Veereshlingam et al. 2004; Bourcy et al. 2013; Sinharoy et al. 2013; Berrabah et al. 2014; Wang et al. 2016; Pislariu et al. 2019). Similar to these genes, *AeORM1* is likely to be important in preventing inappropriate activation of defense-like responses during nodulation. It will be of interest to investigate the transcriptional reprogramming in *orm1* mutant bumps and specify the defense-related pathways that

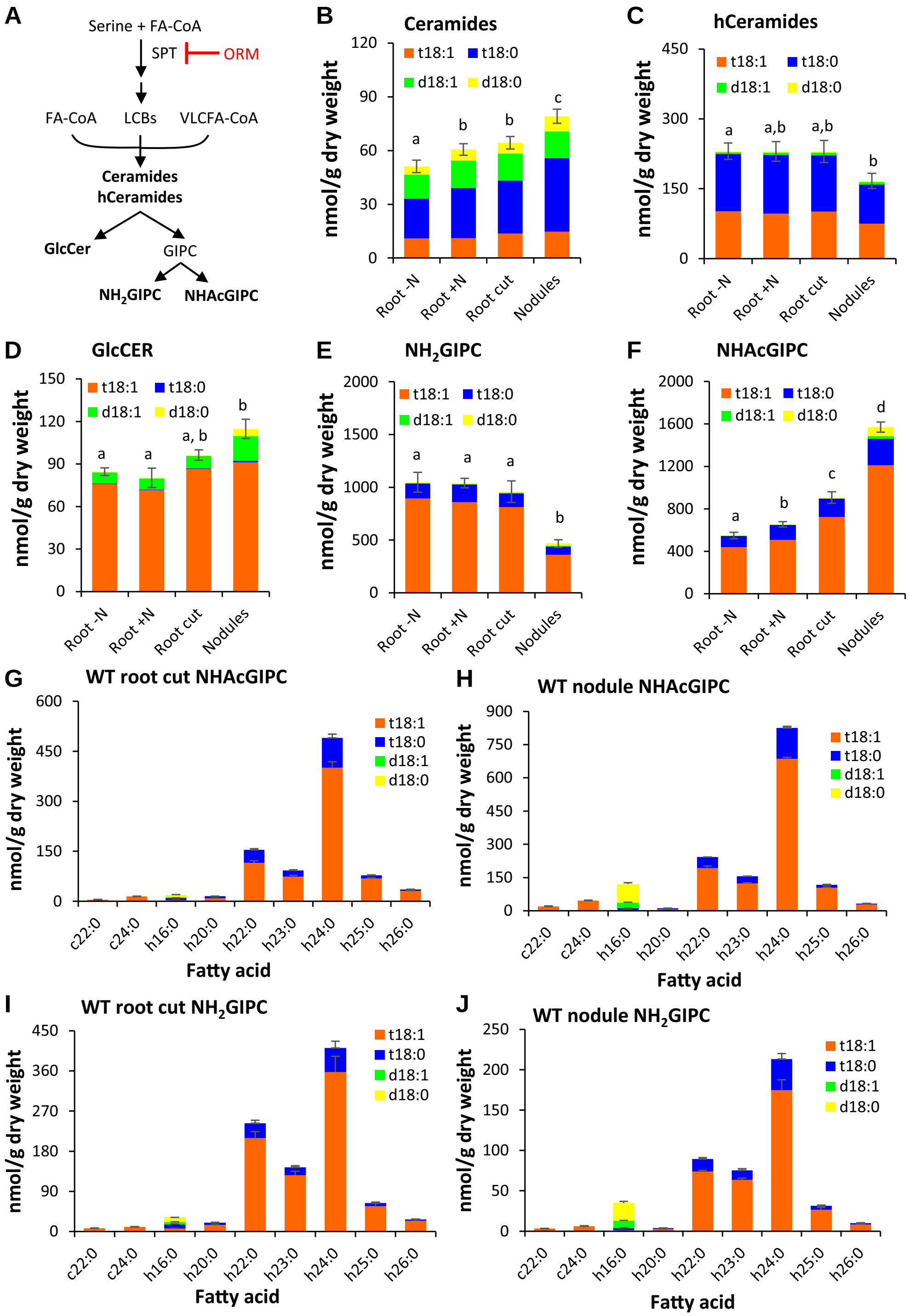

Figure 9. Sphingolipid profiling of the roots and nodules of WT *A. evenia*. **A)** Simplified sphingolipid synthesis pathway with the negative regulation of ORM proteins on the SPT. Arrows indicate steps of the biosynthetic pathway, and the bar indicates the negative regulation of ORM proteins. **B to F)** Content of the following sphingolipid classes in roots and nodules of the WT plants after inoculation with *Bradyrhizobium* ORS278: **B**) CER, **C**) hCeramides, **D**) GlcCER, **E**) NH2GIPC, and **F**) NHAcGIPC. Root − N: roots in BNM with 0.5 mM KNO3. Root + N: roots in BNM medium with 5 mM KNO3. Root cut: inoculated roots from which nodules were removed. The LCB structures present in the analyzed sphingolipids were as follows: d18:0, d18:1, t18:0, and t18:1. **G to J)** Comparison of NHAcGIPC and NH_2GIPC molecular species composition between the WT roots and nodules after inoculation with *Bradyrhizobium* ORS278. **G, H)** NHAcGIPC molecular species in WT roots after removal of nodules **G)** and in nodules **H)**. **I, J)** NH_2GIPC molecular species in WT roots after removal of nodules **I)** and in nodules **J)**. Values are means ± SD from 3 technical replicates. The experiments were performed twice with similar results. The result of 1 representative experiment is shown. Statistical analyses were performed to compare sphingolipid contents in different conditions in the WT line **B to F)**. In that case, different letters represent significant differences between total amounts of considered sphingolipids determined using a Welch's *t*-test, $P < 0.05$. FA, fatty acid; hCeramide, hydroxyceramide; GlcCER, Glucosylceramide; GIPC, glycosyl inositolphosphoceramide; NH_2GIPC, amino-GIPC; NHAcGIPC, acetyl-amino-GIPC.

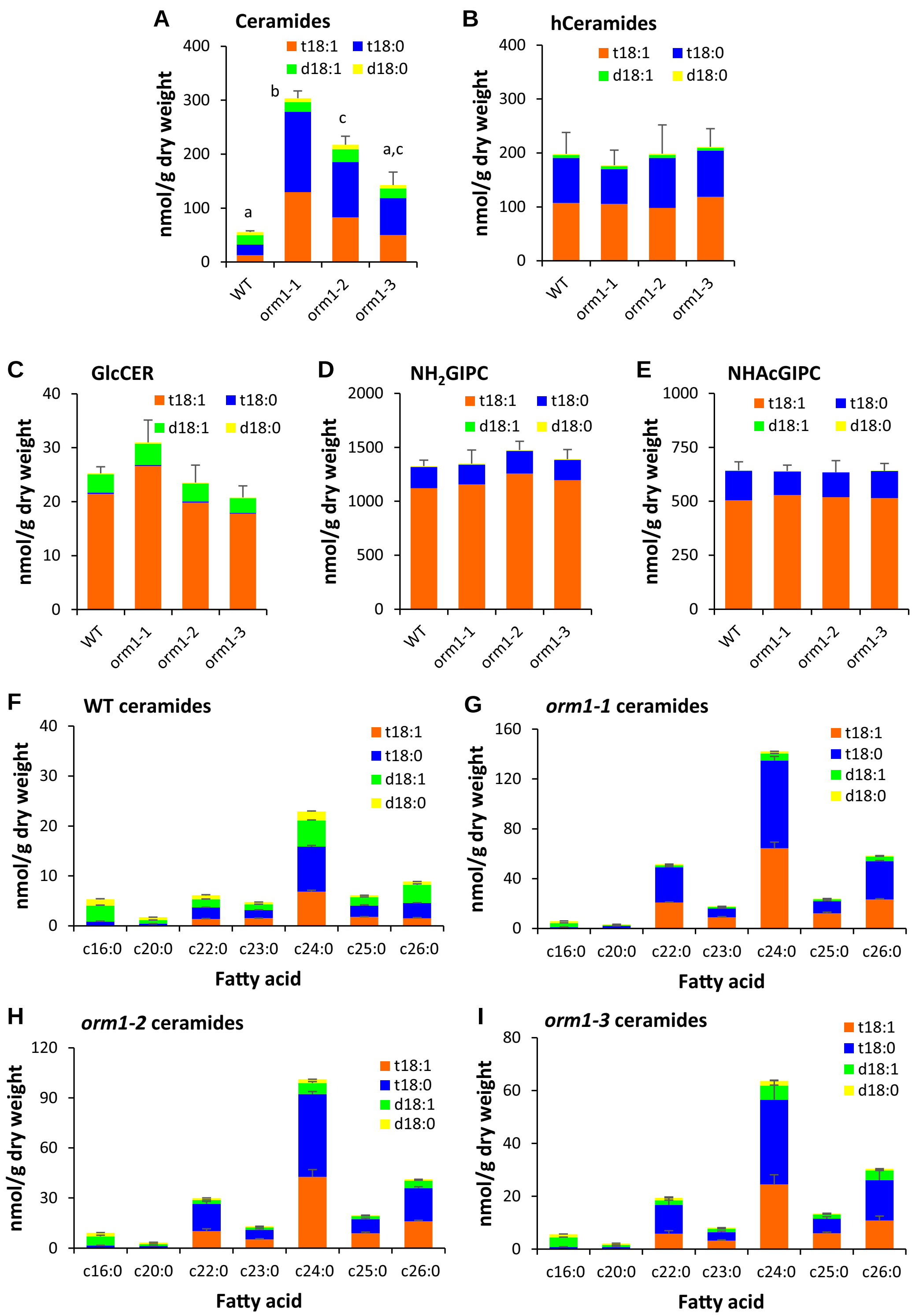

Figure 10. Mutations in *AeORM1* cause sphingolipid accumulation in the root. **A to E)** Content of the following sphingolipid classes in roots and nodules of the WT plants after inoculation with *Bradyrhizobium* ORS278: **A)** CER, **B)** hCeramides, **C)** GlcCER, **D)** NH2GIPC, and **E)** NHAcGIPC. Root − N: roots in BNM medium with 0.5 mM KNO3. Root + N: roots in BNM medium with 5 mM KNO3. Root cut: inoculated roots from which nodules were removed. The LCB structures present in the analyzed sphingolipids were as follows: d18:0, d18:1, t18:0, and t18:1. **F to I)** CER molecular species composition representing the exact pairings of LCB and fatty acid in roots of WT and *orm1* mutant plants. **F)** WT, **G)** *orm1-1* mutant, **H)** *orm1-2* mutant, and **I)** *orm1-3* mutant. Values are means ± SD from 3 technical replicates. The experiments were performed twice with similar results. The result of 1 representative experiment is shown. Statistical analyses were performed to compare sphingolipid contents between the WT and *orm1* mutant lines **A to E)**. In that case, different letters represent significant differences between total amounts of considered sphingolipids determined using a Welch's *t*-test, $P < 0.05$.

are activated by inoculation with *Bradyrhizobium*. Although aborted nodules with defense-like reactions were the most striking phenotype among *A. evenia orm1* mutants, paying closer attention also revealed an alteration in lateral root formation, with all 3 mutants having lateral roots shorter as compared to WT plants. Such defect was not seen in other *A. evenia* nodulation mutants for *AeCCaMK* and *AeNSP2* (this study; Quilbé, Nouwen, et al. 2022), confirming the idea that this phenotype is specific to mutations in *AeORM1*. In accordance, *AeORM1* is specifically expressed in lateral root primordia and apex (prior and after emergence, respectively) in nonsymbiotic conditions. Taken together, phenotypic and expression data for *AeORM1* establish a link between nodule and lateral root formation. Only a few genes shared between lateral root development and nodule formation are known, which include the aforementioned *MtNIP/LATD* gene that encodes a nitrate transporter (Yendrek et al. 2010; Bagchi et al. 2012) and *LBD16* (LOB-DOMAIN PROTEIN 16) coding for a transcription factor that acts with NF-YA1 to promote auxin signaling (Schiessl et al. 2019; Soyano et al. 2019). Although no role of ORM proteins in lateral root development has been described in nonlegume plants, it is tempting to speculate that this developmental function has been co-opted for nodulation in legumes as for *MtNIP/LATD* and *LBD16*.

Given the very high identity level of ORM proteins from legume and nonlegume species, it is likely that ORM function is very conserved. ORM proteins are ER-resident membrane proteins that negatively regulate sphingolipid metabolism by forming a multiprotein complex with SPT. Tight regulation of sphingolipid homeostasis is critical since sphingolipids can act as bioactive molecules and are incorporated into cell membranes, influencing their structural and functional dynamics, especially vesicular trafficking, endocytosis and exocytosis. Therefore, they impact cell polarization, lipid raft formation, protein targeting to the membrane, and also cell cytokinesis. We found that mutations in *AeORM1* primarily affected CER synthesis and composition in *A. evenia* roots leading to the accumulation of mainly VLCFA-containing CER species (C22 to C26). In *Arabidopsis*, *ORM* gene inactivation also leads to the increase of CER content, but this concerns the CER backbones containing long-chain fatty acids (C16) rather than those with VLCFAs (Kimberlin et al. 2016; Li et al. 2016). These opposed data point to a differential impact of ORM mediation of SPT activity on CER synthase activities between *A. evenia* and *Arabidopsis*. These regulatory differences may be of importance in legume biology because VLCFAs and VLCFA-containing sphingolipids play a key role in cell proliferation, tissue patterning, and lateral root development (Roudier et al. 2010; Trinh et al. 2019; Nagata et al. 2021). This suggests that a fine-tuning of VLCFA-CER content in *A. evenia* may be essential for the correct development of lateral roots and nodules. Furthermore, VLCFA-containing sphingolipids have been demonstrated to associate with Golgi-mediated protein trafficking in *Arabidopsis* (Markham et al. 2011). The inactivation of ORM function may notably impact certain membrane-anchored proteins that intervene in the rhizobial symbiosis, such as the Golgi-located VPY (Liu et al. 2019). However, this ORM regulation of the sphingolipid biosynthesis during nodule symbiosis remains to be investigated. Recent work in *M. truncatula* revealed that sphingolipids are also important for bacterial accommodation as they are part of the plant-produced membrane delimiting symbiosomes containing the bacteria. Bacterial accommodation is linked to the reprogramming of sphingolipid glycosylation (Moore et al. 2021). In *A. evenia*, a similar change in sphingolipid glycosylation between roots and nodules was shown here, indicating that this process may be a general rule in legumes. These changes were shown to be mediated by *MtGINT1* (Glucosamine Inositol Phosphorylceramide Transferase 1) whose inactivation impaired nodulation and mycorrhization. In *A. evenia*, a similar change in sphingolipid glycosylation between roots and nodules was shown here, indicating that this process may be a general rule in legumes. In contrast to *M. truncatula gint1* silenced lines, *A. evenia orm1* mutants were not impaired in mycorrhizal symbiosis. This does not exclude an involvement of *ORM* genes in mycorrhization since a second *ORM* gene is present in *A. evenia*, *AeORM2*, and it could intervene in this symbiosis, either alone or redundantly with *AeORM1*. Resolving this question, determining the precise cellular function of ORM-regulated sphingolipid homeostasis in nodule formation, and how it relates to lateral root formation represent important avenues in the research to uncover the mechanisms of symbiotic infection and LRB nodulation in *A. evenia* and the rhizobial symbiosis in legumes in general.

Materials and methods

Plant materials and growth conditions

In this study, *A. evenia* CIAT22838 was used as a WT reference plant and in some experiments its *ccamk*-3 mutant as negative control (Quilbé et al. 2021; Quilbé, Nouwen, et al. 2022). All analyzed *orm* mutants were isolated from the EMS-mutagenized collection of *A. evenia* CIAT22838 plants that have been shown to have phenotypic defects in nodulation (Quilbé et al. 2021). *A. evenia* seeds were scarified for 40 min with sulfuric acid (96%) and rinsed several times with distilled water; whereafter, germination was induced by overnight incubation in distilled water containing 0.01% (v/v) ethrel (BAYER). For root phenotyping and seed production, 1-d-old seedlings were transferred to plastic pots filled with attapulgite hereafter the plants were cultivated in the greenhouse (28 °C and 70% relative humidity) as detailed in Quilbé et al. (2021).

Analysis of the root system architecture

Plants were cultured in tubes filled with BNM as published (Quilbé, Nouwen, et al. 2022). Roots were scanned using an EPSON GT-15000 scanner, and measurements of root length or density were performed using the Optimas 6.1 software (Media Cybernetics, Silver Spring, MD, USA).

Plant nodulation and acetylene reduction assays

For analysis of rhizobial infection and nodulation, *Bradyrhizobium* WT strain ORS278 and the derivative strains ORS278-GUS or ORS278-GFP were used (Giraud et al. 2007; Bonaldi et al. 2011). In each case, nodulation tests were performed in covered tubes to protect roots from light. Bacterial culture, root inoculation, nitrogenase enzyme activity (through the measurement of acetylene reducing activity [ARA]), and macroscopic observations were performed as already published (Bonaldi et al. 2011; Arrighi et al. 2012; Quilbé, Nouwen, et al. 2022).

For confocal microscopy, root sections containing nodules from plants inoculated with ORS278-GFP were harvested and rinsed with distilled water. The rinsed root sections were embedded in 5% agar (w/v) and sectioned (70 μM) using a vibratome (VT1000S; Leica, Nanterre, France). Images of nodule section were taken with a Carl Zeiss LSM 700 (Jen, Germany) confocal microscope using the following laser excitation/emission cutoffs: 493 to 525 nm (GFP: intensity 5% to 11%; gain: 500 to 750) and 555/560 to 630 nm (autofluorescence: 6% to 11%; gain: 500 to 800). Obtained images were analyzed and processed using the ZEN software supplied with the confocal microscope.

Plant mycorrhization

Mycorrhization tests were performed by inoculating 5-d-old *A. evenia* seedlings with *R. irregularis* DAOM197198 (Agronutrition, Carbonne, France) and by optimizing culture conditions described in Quilbé, Nouwen, et al. (2022). In short, plants were watered 3 times a week with the nutritive solution, trays containing pots with plants were changed weekly, and plants were cultured for 6 wk following inoculation with spores. Fungal colonization was assessed on 6 plants/genotype/biological repeat using the Myco-Calc method as detailed in Quilbé, Nouwen, et al. (2022).

Histochemical staining

Bacterial infection of plant tissue and nodule development were analyzed using 70-μm-thick vibratome (Leica VT1000S) sections of freshly harvested material. In case of inoculation with strain ORS278-GUS, sections were stained with X-Gluc (Fabre et al. 2015). Root sections were observed using a Nikon DS-Ri2 microscope either under bright field illumination or using the GFP and mCherry filters to analyze autofluorescence. To estimate H_2O_2 production in situ, root and nodule sections were immersed in 1 mg.mL^{-1} of DAB solution, vacuum infiltrated for 2 min, and then incubated for 2 to 3 h at 25 °C before observation. The accumulation of phenolic compounds was detected by potassium permanganate–methylene blue staining as described (Bourcy et al. 2013).

Genetic characterization and sequencing of *A. evenia* mutants

For the genetic determinism analysis of nodulation mutants, plants were manually hybridized with the WT line. Approximately 600 plants of the mutant × WT F_2 progeny were cultured in the greenhouse, inoculated with the *Bradyrhizobium* strain ORS278, and roots were phenotyped 4 wk after inoculation. For each nodulation mutant, DNA was extracted from pooled roots of 95 to 150 F_2 plants with a mutant phenotype using the CTAB method. Library preparation and sequencing on a NovaSeq sequencer were performed at the Norwegian Sequencing Center (CEES, Oslo, Norway). The 150-bp paired-end reads were processed to conduct the mapping-by-sequencing approach to identify candidate genes as previously described (Quilbé et al. 2021). Allelism tests were performed by directed crossing of the nodulation mutants and root phenotyping of the F_1 progeny cultured either in the greenhouse or growth chamber and inoculated with the *Bradyrhizobium* strain ORS278. Genetic characteristics of the mutants are provided in Supplemental Tables S1 and S2.

In silico gene analysis

Genes homologous to *AeORM1* were identified in legume species by mining the orthogroups database generated with OrthoFinder (Quilbé et al. 2021). The data set was completed by searching for other legume genes as well as *Arabidopsis* and rice *ORM* genes in the Legume Information System (https://www.legumeinfo.org), The Arabidopsis Information Resource (https://www.arabidopsis.org), and the Rice Genome Annotation Project (http://rice.uga.edu) databases, respectively. A maximum likelihood phylogenetic tree reconstruction was obtained by aligning nucleotide sequences with the MUSCLE program that is incorporated in the MEGA X (v10.1.8) software. Aligned sequences were further processed in MEGA X using the maximum likelihood approach and the Kimura 2-parameter model with a 1,000× bootstrap. The data are presented as a rooted tree using rice as an outgroup. For the *AeORM1* and *AeORM2* genes, microsynteny analysis was performed using the Legume Information System with the Genome Context Viewer (https://legumeinfo.org/lis_context_viewer) to visualize the gene collinearity in syntenic regions and their expression patterns were obtained using the *A. evenia* Gene Atlas available at the AeschynomeneBase (http://aeschynomenebase.fr/content/gene-expression).

Protein sequences were aligned using the MUSCLE program in the MEGA X software and sequence alignments were visualized with Jalview v2.11.0. AeORM1 protein domains were identified, annotated using InterProscan (http://www.ebi.ac.uk/interpro/) and DeepTMHMM (https://dtu.biolib.com/DeepTMHMM), and refined by comparative structural analysis with other *Arabidopsis* ORM proteins. AA conservation and properties were further analyzed with WebLogo3 (https://weblogo.threeplusone.com).

Constructs for in planta gene analyses

For the analysis of the *AeORM1* gene, different constructs were generated based on the Golden Gate cloning method using vectors and modules generated by Fliegmann et al. (2016). In the first step, sequences of the *AeORM1* 2.166-bp native promoter (pro*AeORM1*) and of the full-length CDS of *AeORM1* containing the stop codon were flanked by 2 *Bsa*I sites designated so as to generate specific cohesive 5′ protruding ends (Supplemental Table S4). These sequences were synthesized and cloned into Puc57-*Bsa*I-free plasmid by GeneCust (www.genecust.com) and checked by DNA sequencing. For *A. evenia* root transformation, the cloned promoter pro*AeORM1* was fused to the *GUS* gene and the full-length CDS *AeORM1* with stop codon by Golden Gate cloning, using a vector based on pCambia2200 expressing DsRED.

Functional complementation experiment

Using *A. rhizogenes*-mediated transformation (Quilbé et al. 2021), seedlings of *orm1-1* were transformed using ARqua1 strains containing either empty vector or ProAeORM1: AeORM1 construct in pCambia2200DsRED. Plants were initially cultured on agar plates with half-strength MS medium (MS basal salt mixture). After 3 wk of growth, transformed roots were identified by expression of the DsRed marker, and nontransformed ones were removed from the plants. Subsequently, plants were transferred to Falcon tubes filled with liquid BNM and inoculated with the *Bradyrhizobium* strain ORS278. Nodulation was quantified 28 d after inoculation. The number of nodulated plants out of the total transformed plants and the number of nodules per nodulated plant were determined.

Analysis of promoter-GUS expressing plants

The pCambia2200DsRED vector containing the proAeORM1-GUS fusion was transformed into *A. rhizogenes* strain ARqua1, and cells harboring this plasmid were used to transform WT *A. evenia* as described (Quilbé et al. 2021). Plants developing transformed roots were selected as described above. The *AeORM1* promoter activity was analyzed in noninoculated roots and at different times after inoculation with the *Bradyrhizobium* strain ORS278. Untransformed WT seedlings were used as a negative control. Whole roots and 70-μm-thick nodule sections (obtained with a Leica VT1000S vibratome, Nanterre, France) were stained with X-Gluc (Fabre et al. 2015). Images of GUS-analyzed tissues were taken with a stereo macroscope (Niko AZ100, Champigny-sur-Marne, France) using the Nikon Advanced software.

RNA isolation and RT-qPCR

For expression analysis of *AeORM1* and *AeORM2*, RNA material that has been previously generated in biological triplicates for the WT line in noninoculated conditions or inoculated either with *Bradyrhizobium* strain ORS278 or with *R. irregularis* DAOM197198 was used (Quilbé, Nouwen, et al. 2022). For expression analysis of symbiotically induced genes, pools of 5 roots were collected per genotype and time point to serve as a source of RNA material. They were obtained across 4 independent experiments. For the total RNA extraction from roots, RT-qPCR was performed as described (Fabre et al. 2015; Gully et al. 2018).. Expression levels were normalized with the *AeEF1-α* and *AeUbi* reference genes. Gene-specific primers were designed with Beacon Designer (Premier Biosoft) (Supplemental Table S5).

Sphingolipid extraction and analysis

For root sphingolipid analysis, roots from 4-wk-old plants grown in liquid BNM (supplemented with 0.5 or 5 mmol KNO_3) were harvested and 3 pools of 3 roots were formed. For nodule sphingolipid analysis, nodulated roots of plants inoculated with *Bradyrhizobium* ORS278 were collected at 4 wpi and nodules were separated from 10 roots to constitute 3 bulks of roots and nodules, respectively. The experiments were performed twice. Sphingolipids were extracted from 6 to 10 mg of lyophilized plant material as described previously (Tellier et al. 2014). Here, 1 mL of extraction solvent (isopropanol:hexane:water, 55:20:25) and 10 μL of adequate internal standards were added to 2 mg of freeze-dried material and grinded using a Polytron homogenizer. The sample was incubated at 60 °C for 15 min. After centrifugation at 1,620 × *g* for 5 min, the supernatant was recovered and the pellet was extracted once more with 1 mL of extraction solvent as previously. Supernatants were combined and dried using a Speed-Vac evaporator. To improve ionization, the samples were subjected to alkaline hydrolysis, whereafter they were resuspended in 100 μL of tetrahydrofuran (THF):methanol:water (2:1:2) containing 0.1% (v/v) formic acid (for GIPCs classes and GlcCERs) or THF (for CERs and hCERs) by sonication and filtrated before analysis. Sphingolipid standards used were GM1 (20 nmol), C12-GlcCER (10 nmol), and C12-CER (1 nmol) in 1 mL of extraction solvent (isopropanol:hexane:water, 55:20:25). They were purchased from AvantiPolar Lipids, Inc. (Alabaster, AL, USA). Ultrahigh-performance liquid chromatography (UPLC)-electrospray ionization (ESI)-tandem MS (MS/MS) analyses were carried out on a Waters Acquity UPLC system coupled to a Waters Xevo tandem quadrupole mass spectrometer (Manchester, UK) equipped with an ESI source. The mass analyses were performed in the positive multiple reaction monitoring mode. Chromatographic conditions and mass spectrometric parameters were defined previously (Tellier et al. 2014).

Statistical analyses

To evaluate statistically the monogenic determinism of the 3 *orm1* mutants, a Student's *t*-test was performed. A Mann–Whitney test was used to compare gene expression levels in the WT and *orm1-1* lines. One-way Kruskal–Wallis analysis was performed to compare root parameters between the WT line and the 3 *orm1* mutants. Values of $P < 0.05$ were considered statistically significant. A Welch's *t*-test was used to compare sphingolipid levels between *orm1* mutants and the WT line. The statistical analyses were done using the R package or GraphPad Prism 8.3.0.

Accession numbers

The mapping-by-sequencing data generated for the *orm1* mutant in this study were deposited in the NCBI database under BioProject ID: PRJNA727694. Accession numbers for the *A. evenia* genes studied in this work are as follows: *AeORM1* (Ae02g01550), *AeORM2* (Ae06g10480), *AeENOD40* (Ae03:4310314..4311019), *AeSymREM1* (Ae03g30480), *AeVPY* (Ae05g16930), *AeCRK* (Ae05g12380), *AeSBT* (Ae05g09230), *AeNIN* (Ae07g00100), *AeRAM1* (Ae06g18380), *AeSBTM1* (Ae05g09240), *AeSTR* (Ae05g35200), *AePT4* (Ae08g08360), *AeEF1a* (Ae09g20140), and *AeUbi* (Ae10g10900). Corresponding sequence data can be found in the AeschynomeneBase (http://aeschynomenebase.fr/) or Legume Information System (https://www.legumeinfo.org/) databases.

Acknowledgments

We thank Robin Duponnois (LSTM Laboratory, IRD) for assistance with the characterization of *A. evenia* nodulation mutants and for kindly providing fungi spores for mycorrhization experiments. We also thank Benoit Lefebvre (LIPME Laboratory, INRAE) for providing the pCambiaRedGG plasmid for Golden Gate cloning.

Author contributions

N.N., F.G., and J.-F.A. conceived and designed the experiments; N.N., M.P., F.E.M., F.T., M.R., N.H.A., C.K., F.G., and J.-F.A. performed the experiments and analyzed the data; and N.N., F.G., and J.-F.A. wrote the article.

Supplemental data

The following materials are available in the online version of this article.

Supplemental Figure S1. Identification of *orm1* mutant alleles by mapping-by-sequencing.

Supplemental Figure S2. Syntenic localization of *ORM* genes in *A. evenia*.

Supplemental Figure S3. Structure and alignment of plant ORM proteins.

Supplemental Figure S4. *AeORM1* and *AeORM2* are expressed throughout the plant.

Supplemental Figure S5. Nodulation kinetics of the WT and *orm1* mutant plants after inoculation with *Bradyrhizobium* ORS278.

Supplemental Figure S6. Mutations in *AeORM1* generate autofluorescence.

Supplemental Figure S7. Characterization of the mycorrhizal phenotype in the *orm1* mutants.

Supplemental Table S1. Genetic data of the *A. evenia orm1* mutants.

Supplemental Table S2. Allelism analysis of the *A. evenia orm1* mutants.

Supplemental Table S3. Complementation of the nodulation phenotype of *orm1-1* mutant plants by expressing WT *AeORM1*.

Supplemental Table S4. Sequences used for Golden Gate cloning.

Supplemental Table S5. Primer sequences used for RT-qPCR.

Funding

This work was supported by the French National Research Agency (ANR-SymWay-21-CE20-0011-01) and the French Institut National de Recherche pour l'Agriculture, l'Alimentation et l'Environnement (INRAE) (SPE project "Sym Interface" AAP 2022).

Conflict of interest statement. None declared.

Data availability

All data are incorporated into the article and its online supplementary material.

References

Alsiyabi A, Solis AG, Cahoon EB, Saha R. Dissecting the regulatory roles of ORM proteins in the sphingolipid pathway of plants. PLoS Comput Biol. 2021:**17**(1):e1008284. https://doi.org/10.1371/journal.pcbi.1008284

Arrighi JF, Cartieaux F, Brown SC, Rodier-Goud M, Boursot M, Fardoux J, Patrel D, Gully D, Fabre S, Chaintreuil C, et al. *Aeschynomene evenia*, a model plant for studying the molecular genetics of the nod-independent rhizobium-legume symbiosis. Mol Plant Microbe Interact. 2012:**25**(7):851–861. https://doi.org/10.1094/MPMI-02-12-0045-TA

Bagchi R, Salehin M, Adeyemo OS, Salazar C, Shulaev V, Sherrier DJ, Dickstein R. Functional assessment of the *Medicago truncatula* NIP/LATD protein demonstrates that it is a high-affinity nitrate transporter. Plant Physiol. 2012:**160**(2):906–916. https://doi.org/10.1104/pp.112.196444

Berrabah F, Bourcy M, Eschstruth A, Cayrel A, Guefrachi I, Mergaert P, Wen J, Jean V, Mysore KS, Gourion B, et al. A nonRD receptor-like kinase prevents nodule early senescence and defense-like reactions during symbiosis. New Phytol. 2014:**203**(4):1305–1314. https://doi.org/10.1111/nph.12881

Berrabah F, Ratet P, Gourion B. Legume nodules: massive infection in the absence of defense induction. Mol Plant Microbe Interact. 2019:**32**(1):35–44. https://doi.org/10.1094/MPMI-07-18-0205-FI

Bhattacharjee O, Raul B, Ghosh A, Bhardwaj A, Bandyopadhyay K, Sinharoy S. Nodule INception-independent epidermal events lead to bacterial entry during nodule development in peanut (*Arachis hypogaea*). New Phytol. 2022:**236**(6):2265–2281. https://doi.org/10.1111/nph.18483

Bonaldi K, Gargani D, Prin Y, Fardoux J, Gully D, Nouwen N, Goormachtig S, Giraud E. Nodulation of *Aeschynomene afraspera* and *A. indica* by photosynthetic *Bradyrhizobium* sp. strain ORS285: the Nod-dependent versus the nod-independent symbiotic interaction. Mol Plant Microbe Interact. 2011:**24**(11):1359–1371. https://doi.org/10.1094/MPMI-04-11-0093

Bourcy M, Brocard L, Pislariu CI, Cosson V, Mergaert P, Tadege M, Mysore KS, Udvard MK, Gourion B, Ratet P. *Medicago truncatula*

DNF2 is a PI-PLC-XD-containing protein required for bacteroid persistence and prevention of nodule early senescence and defense-like reactions. New Phytol. 2013:**197**(4):1250–1261. https://doi.org/10.1111/nph.12091

Capoen W, Oldroyd G, Goormachtig S, Holsters M. *Sesbania rostrata*: a case study of natural variation in legume nodulation. New Phytol. 2010:**186**(2):340–345. https://doi.org/10.1111/j.1469-8137.2009.03124.x

Chaintreuil C, Perrier X, Martin G, Fardoux J, Lewis GP, Brottier L, Rivallan R, Gomez-Pacheco M, Bourges M, Lamy L, et al. Naturally occurring variations in the Nod-independent model legume *Aeschynomene evenia* and relatives: a resource for nodulation genetics. BMC Plant Biol. 2018:**18**(1):54. https://doi.org/10.1186/s12870-018-1260-2

Fabre S, Gully D, Poitout A, Patrel D, Arrigh JF, Giraud E, Czernic P, Cartieaux F. Nod factor-independent nodulation in *Aeschynomene evenia* required the common plant microbe symbiotic toolkit. Plant Physiol. 2015:**169**(4):2654–2664. https://doi.org/10.1104/pp.15.01134

Feng J, Lee T, Schiessl K, Oldroyd GED. Processing of NODULE INCEPTION controls the transition to nitrogen fixation in root nodules. Science. 2021:**374**(6567):629–632. https://doi.org/10.1126/science.abg2804

Fliegmann J, Jauneau A, Pichereaux C, Rosenberg C, Gasciolli V, Timmers ACJ, Burlet-Schiltz O, Cullimore J, Bono JJ. LYR3, a high-affinity LCO-binding protein of *Medicago truncatula*, interacts with LYK3, a key symbiotic receptor. FEBS Lett. 2016:**590**(10):1477–1487. https://doi.org/10.1002/1873-3468.12191

Giraud E, Moulin L, Vallenet D, Barbe V, Cytryn E, Avarre JC, Jaubert M, Simon D, Cartieaux F, Prin Y, et al. Legumes symbioses: absence of *Nod* genes in photosynthetic bradyrhizobia. Science. 2007:**316**(5829):1307–1312. https://doi.org/10.1126/science.1139548

Gobbato E. Recent developments in arbuscular mycorrhizal signaling. Cur Opin Plant Biol. 2015:**26**:1–7. https://doi.org/10.1016/j.pbi.2015.05.006

Gonzalez-Solis A, Han G, Gan L, Li Y, Markham JE, Cahoon E, Dunn TM, Cahoon EB. Unregulated sphingolipid biosynthesis in gene-edited *Arabidopsis* ORM mutants results in nonviable seeds with strongly reduced oil content. Plant Cell. 2020:**32**(8):2474–2490. https://doi.org/10.1105/tpc.20.00015

Gully D, Czernic P, Cruveiller S, Mahé F, Longin C, Vallenet D, François P, Nidelet S, Rialle S, Giraud E, et al. Transcriptome profiles of Nod factor-independent symbiosis in the tropical legume *Aeschynomene evenia*. Sci Rep. 2018:**8**(1):10934. https://doi.org/10.1038/s41598-018-29301-0

Hossain MS, Shrestha A, Zhong S, Miri M, Austin RS, Sato S, Ross L, Huebert T, Tromas A, Torres-Jerez I, et al. *Lotus japonicus* NF-YA1 plays an essential role during nodule differentiation and targets members of the SHI/STY gene family. Mol Plant Microbe Interact. 2016:**29**(12):950–964. https://doi.org/10.1094/MPMI-10-16-0206-R

Kimberlin AN, Han G, Chen M, Cahoon RE, Luttgeharm KD, Stone JM, Markham JE, Dunn TM, Cahoon EB. ORM expression alters sphingolipid homeostasis and differentially affects ceramide synthase activity. Plant Physiol. 2016:**172**(2):889–900. https://doi.org/10.1104/pp.16.00965

Lace B, Su C, Invernot Perez D, Rodriguez-Franco M, Vernié T, Batzenschlager M, Egli S, Liu CW, Ott T. RPG acts as a central determinant for infectosome formation and cellular polarization during intracellular rhizobial infections. eLife. 2023:**12**:e80741. https://doi.org/10.7554/eLife.80741

Laporte P, Lepage A, Fournier J, Catrice O, Moreau S, Jardinaud MF, Mun JH, Larrainzar E, Cook DR, Gamas P, et al. The CCAAT box-binding transcription factor NF-YA1 controls rhizobial infection. J Exp Bot. 2014:**65**(2):481–494. https://doi.org/10.1093/jxb/ert392

Li J, Yin J, Rong C, Li KE, Wu JX, Huang LQ, Zeng HY, Sahu SK, Yao N. Orosomucoid proteins interact with the small subunit of serine palmitoyltransferase and contribute to sphingolipid homeostasis and stress responses in *Arabidopsis*. Plant Cell. 2016:**28**(12):3038–3051. https://doi.org/10.1105/tpc.16.00574

Li QG, Zhang L, Li C, Dunwell JM, Zhan YM. Comparative genomics suggests that an ancestral polyploidy event leads to enhanced root nodule symbiosis in the Papilionoideae. Mol Biol Evol. 2013:**30**(12):2602–2611. https://doi.org/10.1093/molbev/mst152

Liu CW, Breakspear A, Stacey N, Findlay K, Nakashima J, Ramakrishnan K, Liu M, Xie F, Endre G, de Carvalho-Niebel F, et al. A protein complex required for polar growth of rhizobial infection threads. Nat Commun. 2019:**10**(1):2848. https://doi.org/10.1038/s41467-019-10029-y

Markham JE, Molino D, Gissot L, Bellec Y, Hématy K, Marion J, Belcram K, Palauqui JC, Satiat-Jeunemaître B, Faure JD. Sphingolipids containing very-long-chain fatty acids define a secretory pathway for specific polar plasma membrane protein targeting in *Arabidopsis*. Plant Cell. 2011:**23**(6):2362–2378. https://doi.org/10.1105/tpc.110.080473

Miyata K, Kawaguchi M, Nakagawa T. Two distinct EIN2 genes cooperatively regulate ethylene signaling in *Lotus japonicus*. Plant Cell Physiol. 2013:**54**(9):1469–1477. https://doi.org/10.1093/pcp/pct095

Moore W, Chan C, Ishikawa T, Rennie EA, Wipf HML, Benites V, Kawai-Yamada M, Mortimer JC, Scheller HV. Reprogramming sphingolipid glycosylation is required for endosymbiont persistence in *Medicago truncatula*. Curr Biol. 2021:**31**(11):2374–2385.e4. https://doi.org/10.1016/j.cub.2021.03.067

Nagata K, Ishikawa T, Kawai-Yamada M, Takahashi T, Abe M. Ceramides mediate positional signals in *Arabidopsis thaliana* protoderm differentiation. Development. 2021:**148**(2):dev194969. https://doi.org/10.1242/dev.194969

Pislariu CI, Sinharoy S, Torres-Jerez I, Nakashima J, Blancaflor EB, Udvardi MK. The nodule-specific PLAT domain protein NPD1 is required for nitrogen-fixing symbiosis. Plant Physiol. 2019:**180**(3):1480–1497. https://doi.org/10.1104/pp.18.01613

Quilbé J, Lamy L, Brottier L, Leleux P, Fardoux J, Rivallan R, Benichou T, Guyonnet R, Becana M, Villar I, et al. Genetics of nodulation in *Aeschynomene evenia* uncovers mechanisms of the rhizobium-legume symbiosis. Nat Commun. 2021:**12**(1):829. https://doi.org/10.1038/s41467-021-21094-7

Quilbé J, Montiel J, Arrighi JF, Stougaard J. Molecular mechanisms of intercellular rhizobial infection: novel findings of an ancient process. Front Plant Sci. 2022:**13**:922982. https://doi.org/10.3389/fpls.2022.922982

Quilbé J, Nouwen N, Pervent M, Guyonnet R, Cullimore J, Gressent F, Araújo NH, Gully D, Klopp C, Giraud E, et al. A mutant-based analysis of the establishment of Nod-independent symbiosis in the legume *Aeschynomene evenia*. Plant Physiol. 2022:**190**(2):1400–1417. https://doi.org/10.1093/plphys/kiac325

Roudier F, Gissot L, Beaudoin F, Haslam R, Michaelson L, Marion J, Molino D, Lima A, Bach L, Morin H, et al. Very-long-chain fatty acids are involved in polar auxin transport and developmental patterning in *Arabidopsis*. Plant Cell. 2010:**22**(2):364–375. https://doi.org/10.1105/tpc.109.071209

Roy S, Liu W, Nandety RS, Crook A, Mysore KS, Pislariu CI, Frugoli J, Dickstein R, Udvardi MK. Celebrating 20 years of genetic discoveries in legume nodulation and symbiotic nitrogen fixation. Plant Cell. 2020:**32**(1):15–41. https://doi.org/10.1105/tpc.19.00279

Schiessl K, Lilley JLS, Lee T, Tamvakis I, Kohlen W, Bailey PC, Thomas A, Luptak J, Ramakrishnan K, Carpenter MD, et al. NODULE INCEPTION recruits the lateral root developmental program for symbiotic nodule organogenesis in *Medicago truncatula*. Curr Biol. 2019:**29**(21):3657–3668.e5. https://doi.org/10.1016/j.cub.2019.09.005

Sharma V, Bhattacharyya S, Kumar R, Kumar A, Ibañez F, Wang J, Guo B, Sudini HK, Gopalakrishnan S, DasGupta M. Molecular basis of root nodule symbiosis between *Bradyrhizobium* and 'crack-entry' legume groundnut (*Arachis hypogaea* L.). Plants (Basel). 2020:**9**(2):276. https://doi.org/10.3390/plants9020276

Shrestha A, Zhong S, Therrien J, Huebert T, Sato S, Mun T, Andersen SU, Stougaard J, Lepage A, Niebel A, et al. *Lotus japonicus* nuclear factor YA1, a nodule emergence stage-specific regulator of auxin signalling. New Phytol. 2021:**229**(3):1535–1552. https://doi.org/10.1111/nph.16950

Sinharoy S, Torres-Jerez I, Bandyopadhyay K, Kereszt A, Pislariu CI, Nakashima J, Benedito VA, Kondorosi E, Udvardi MK. The C2H2 transcription factor regulator of symbiosome differentiation represses transcription of the secretory pathway gene VAMP721a and promotes symbiosome development in *Medicago truncatula*. Plant Cell. 2013:**25**(9):3584–3601. https://doi.org/10.1105/tpc.113.114017

Soyano T, Shimoda Y, Kawaguchi M, Hayashi M. A shared gene drives lateral root development and root nodule symbiosis pathways in lotus. Science. 2019:**366**(6468):1021–1023. https://doi.org/10.1126/science.aax2153

Tellier F, Maia-Grondard A, Schmitz-Afonso I, Faure JD. Comparative plant sphingolipidomic reveals specific lipids in seeds and oil. Phytochemistry. 2014:**103**:50–58. https://doi.org/10.1016/j.phytochem.2014.03.023

Trinh DC, Lavenus J, Goh T, Boutté Y, Drogue Q, Vaissayre V, Tellier F, Lucas M, Voß U, Gantet P, et al. PUCHI regulates very long chain fatty acid biosynthesis during lateral root and callus formation. Proc Natl Acad Sci U S A. 2019:**116**(28):14325–14330. https://doi.org/10.1073/pnas.1906300116

Veereshlingam H, Haynes JG, Penmetsa RV, Cook DR, Sherrier DJ, Dickstein R. *Nip*, a symbiotic *Medicago truncatula* mutant that forms root nodules with aberrant infection threads and plant defense-like response. Plant Physiol. 2004:**136**(3):3692–3702. https://doi.org/10.1104/pp.104.049064

Wang C, Yu H, Luo L, Duan L, Cai L, He X, Wen J, Mysore KS, Li G, Xiao A, et al. NODULES WITH ACTIVATED DEFENSE 1 is required for maintenance of rhizobial endosymbiosis in *Medicago truncatula*. New Phytol. 2016:**212**(1):176–191. https://doi.org/10.1111/nph.14017

Yano K, Aoki S, Liu M, Umehara Y, Suganuma N, Iwasaki W, Sato S, Soyano T, Kouchi H, Kawaguchi M. Function and evolution of a *Lotus japonicus* AP2/ERF family transcription factor that is required for development of infection threads. DNA Res. 2017:**24**(2):193–203. https://doi.org/10.1093/dnares/dsw052

Yendrek CR, Lee YC, Morris V, Liang Y, Pislariu CI, Burkart G, Meckfessel MH, Salehin M, Kessler H, Wessler H, et al. A putative transporter is essential for integrating nutrient and hormone signaling with lateral root growth and nodule development in Medicago truncatula. Plant J. 2010:**62**(1):100–112. https://doi.org/10.1111/j.1365-313X.2010.04134.x